The Noisy Jackal

Measurement and analysis of the coloured noise on the longitudinal, lateral and rotational velocities and identification of its characteristics due to the unmodeled dynamics of a skid steer mobile robot during a steady-state turning manoeuvre.

A.V. van Doeveren - 1324926

TU**Delft** Delft University of Technology

Department of Cognitive Robotics - Vehicle Engineering

The Noisy Jackal

Measurement and analysis of the coloured noise on the longitudinal, lateral and rotational velocities and identifcation of its characteristics due to the unmodeled dynamics of a skid steer mobile robot during a steady-state turning manoeuvre.

MASTER OF SCIENCE THESIS

For the degree of Master of Science in Vehicle Engineering at Delft University of Technology

A.V. van Doeveren - 1324926

October 28, 2019

Faculty of Mechanical, Maritime and Materials Engineering (3mE) · Delft University of Technology

TUDelft Delft
University of
Technology

Abstract

This research focuses on proving the presence of coloured noise on the longitudinal, lateral and rotational velocity in steady-state cornering of a skid steer mobile robot. Furthermore, it also focuses on the creation of a Gaussian filter which is able to recreate the characteristics of the measured coloured noise. This is done to determine the characteristics of the Gaussian filter based on real-life experimental values, which defines the Gaussian filter that creates coloured process noise in the Active Inference algorithm. To accomplish the main research goal, the following is done:

- Create a linear dynamical model of the jackal robot and optimize the model in such a way that its velocity states resemble the experimental values of the velocities for the given experimental inputs.

- Show the presence of coloured noise in the dynamical behaviour of the jackal robot.

- Create a Gaussian filter and determine its characteristics, which can recreate the coloured noise found in the velocity states of the jackal robot in steady state turning.

To accomplish this, experiments are done capturing the linear acceleration, rotational velocities, position and heading of the skid steer mobile robot using both the internal sensors of the robot as well as an external motion capturing system. A linear model of the jackal robot is constructed and discretised as the noise is a function of the difference between the experimental value for the next step state $[k+1]_{exp}$ and the prediction of the next step state $[k+1]_{est}$. The prediction is made by inputting the experimental values for step $[k]$ into the discretised linear model together with the model input. The difference between $[k+1]_{exp}$ and $[k+1]_{est}$ is the noise on the velocities during the steady-state cornering experiments. Optimal values for Gaussian filter are found by fitting the autocorrelations of coloured noise which is made by filtering white noise with a range of Gaussian filters on the autocorrelation of the measured coloured noise. The result of this research is proof of the presence of coloured noise in skid steer mobile robots which in turn indicates that using Active Inference on these types of robots is a worthwhile approach to control and state estimation.

Table of Contents

Preface

This thesis is the original work of the author Alexander van Doeveren, carried out at the department of Cognitive Robots at the faculty of Mechanical, Maritime and Materials Engineering of TU Delft.

It was a challenging process at times in which I benefited greatly from the support and daily structure of the UNO Club. I would also like to thank my girlfriend Anne, not only for her unfaltering love, patience and moral support but also for giving me the opportunity for pursuing my master's degree, Tim for always standing by with both advice and laughs, my family who never ceased to believe in me, my high-school friends who never got tired of listening to me wailing about my progress and last but not least, my friends and fellow car-enthusiasts at the TU Delft who made the masters degree a far more enjoyable process.

Delft, University of Technology   A.V. van Doeveren - 1324926
October 28, 2019

Acknowledgements

I would like to thank my supervisor prof.dr.ir Martijn Wisse, both for his assistance and guidance during the writing of this thesis, and for the opportunity to develop my skills as supervisor and adviser of a group of mechanical engineering students doing their bachelors thesis.

I would also like to thank Juriaan von Asmuth, Freddy Bos, Max Sibeijn and Laurien Stubbé for their contributions to the experiments performed in this study.

Finally, I would finally like to thank Anne de Groot and Tim Meskers for critically proofreading my thesis.

Delft, University of Technology
October 28, 2019

A.V. van Doeveren - 1324926

Chapter 1

Introduction

Humans are able to learn a wide variety of skills, ranging from very simple tasks as picking up a pen or how to put a pot on a stove without spilling the contents of the pot, mastering musical instruments such as the violin or drums, walking tightropes to driving formula 1 cars at speeds of over 300 km/h to set the fastest time on any given track. Robots on the other hand are in comparison still not very intelligent. A picking task can be taught fairly easily given the right conditions and boundaries, but the self-driving intelligence present on commercially available road cars is nowhere near capable of a fully automated drive from door to door, let alone beating a professional race driver at 300km/h. Improvement is needed in the way robots learn and are being controlled. In search of that improvement, inspiration can even be drawn from the human mind.

Neuroscientist Karl Friston[1] has developed a new approach to artificial intelligence called Active Inference, aptly abreviated as 'AI'. The theory of Active Inference is based on how the hierarchical human brain works which makes it a biologically plausible form of control. The most important aspect of Active Inference for this research is the fact that the algorithm is said to be able to cope with structured noise in a much more efficient and better way than competing algorithms as the Kalman Filter or Optimal Control which are very adequate at controlling away white noise. Structured noise is a type of noise which is not random but has structure to it, as opposed to white noise which is "a uniform mixture of random energy at every frequency"[2]. Structured noise is also known as coloured noise. The structure or colour in the noise can assume all kinds of shapes or colours [2]. Pink or brown noise have a boost in the lower frequencies of the spectrum and a cut in the higher frequencies. This very apparent when listening to pink or brown noise, the noise actually has a lower pitch than white noise. Noise which has a cut in the lower frequencies and a boost in the higher frequencies also exist, this is known as blue or violet noise, which has a higher pitch than white noise, when listening to the noise. An important property of coloured noise for this research is the fact that the noise is correlated with itself which means that autocorrelation is present in the coloured noise, whereas white noise is not correlated with itself.

The fact that Active Inference is able to cope with coloured noise is interesting for real world applications as a lot of disturbances in the real world are not fully random or 'white'. The wind for instance, is such a coloured disturbance. When the wind blows from the west with a velocity of 4 m/s at time $t = 1$, the wind does not suddenly come from the north-east with a velocity of 12 m/s at time $t = 2$. This is just one example of a coloured noise in the real world. A more interesting form of coloured noise in terms of this research is coloured process noise within a physical system.

An example of that is the skidding that occurs when a skid steer mobile robot navigates a course and makes a turn. Due to the nature of locomotion of such a vehicle, whenever a skid steer mobile robot makes a turn, the wheels skid along surface in a varying amount. This highly non-linear dynamical behaviour is very hard to model accurately, which means that it also is hard to control using known techniques. And this is where Active Inference might be of value because Active Inference is said to be very proficient in controlling away coloured noise. This in terms means that, with a known coloured noise, a much more efficient, faster and simpler model of the physical system might suffice in combination with that coloured noise.

1-1   Research goal

This thesis is part of a bigger research on Active Inference and the implementation of Active Inference in real world robots. When this thesis is finalized, it should prove the existence of coloured noise in skid steer mobile robots and thus the need to explore Active Inference as a valid method for control and state estimation for skid steer mobile robots. Taking this into account, the goal of this research is to *Measurement and analysis of the coloured noise on the longitudinal, lateral and rotational velocities and identifcation of its characteristics due to the unmodeled dynamics of a skid steer mobile robot during a steady-state turning manoeuvre.*

Figure 1-1 shows the block scheme of the Active Inference algorithm. The system is depicted in the top part of the block scheme and basically consists of a model with coloured process noise and measurement noise. The bottom part of the block scheme consists of the implementation of the Active Inference algorithm. For this research, the focus lies on the top part of the block scheme. The block that is of most importance in this research is the block H_w which represents the filter which creates the coloured process noise from a source of white noise. The coloured noise present in the skid steer mobile robot is due to the unmodelled dynamics because of its skidding behaviour when turning. Blocks A and B represent the physical system of the skid steer mobile robot and are also of importance in this research.

1-1-1   Research question and sub-question

To accomplish the main goal of this research, three sub-goals can be formulated which will have to be achieved in this report. These sub-goals and sub-questions which stem from the main goal are:
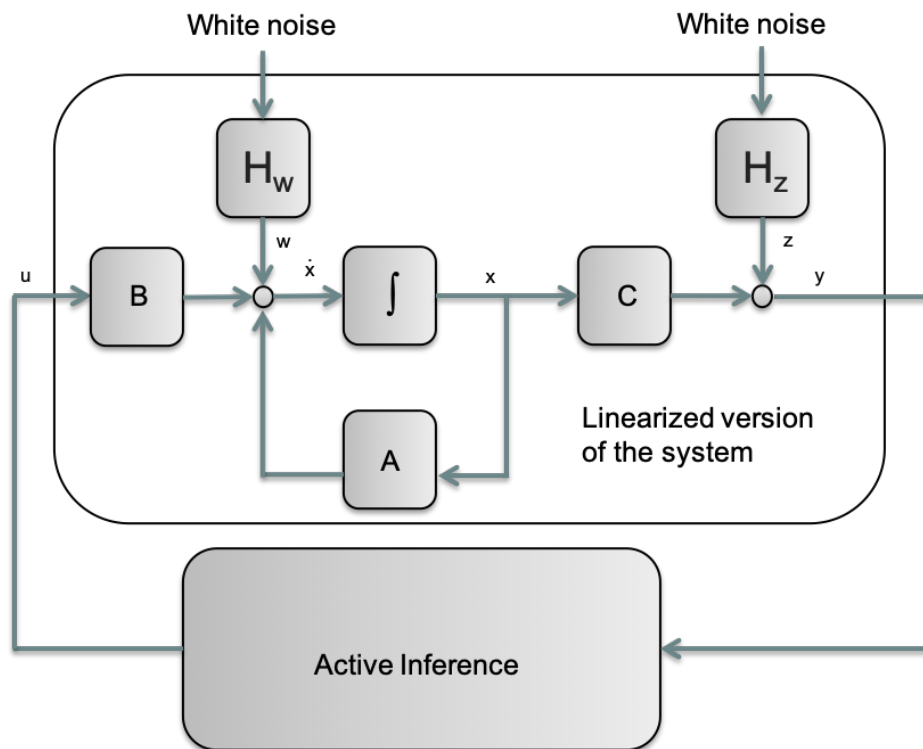
Figure 1-1: Block scheme of the physical system and Active Inference

- Create a linear dynamical model of the jackal robot and optimize the model in such a way that its velocity states resemble the experimental values of the velocities for the given experimental inputs.

- Show the presence of coloured noise in the dynamical behaviour of the jackal robot.

- Create a (Gaussian) filter and determine its characteristics, which can recreate the coloured noise found in the velocity states of the jackal robot in steady state turning.

Chapter 2

Method

This chapter describes the process in this research, the steps that have to be taken and in which order to take those steps to answer the three sub-questions:

- Create a linear dynamical model of the jackal robot and optimise the model in such a way that its velocity states resemble the experimental values of the velocities for the given experimental inputs.

- Show the presence of coloured noise in the dynamical behaviour of the jackal robot.

- Create a (Gaussian) filter and determine its characteristics, which can recreate the coloured noise found in the velocity states of the jackal robot in steady state turning.

Which in turn lead to answering the main goal of this research: *Measurement and analysis of the coloured noise on the longitudinal, lateral and rotational velocities and identifcation of its characteristics due to the unmodeled dynamics of a skid steer mobile robot during a steady-state turning manoeuvre.*

2-1 Process

Experiments are done with a real skid steer mobile robot to obtain real-world data for this research. The skid steer robot in question is the Jackal manufactured by Clearpath Robotics, which is available for use at the department of Cognitive Robotics at 3ME, TU Delft. To objectively track the position and heading of the jackal during the experiments a motion capturing system is used. This motion capturing system is the Optitrack system, which is available to use for the experiments at the Delft Center for System and Control (DCSC) at 3ME, TU Delft. The experiments are designed and executed in such a way that they provide usable data for this research. The experimental setup used for this research can be seen in

Figure 2-1: NERDlab at DCSC, 3ME, TU Delft [3]

Figure 2-1.

Alongside the real-world experiments, the linear dynamical model has to be developed. This model is developed by studying literature to gain information on suitable linear dynamical models of skid steer mobile robots used in other research and by creating a free body diagram of the skid steer mobile robot and performing a dynamical analysis of the system by hand. The resulting linear dynamical model is implemented in MATLAB and is discretised to get a suitable representation of the system which can estimate it's next state using the velocity inputs on the robot and the current state as values for the input of the system.

The next step is to use the real-world experimental data and compare it to the simulation data to gather a definition for the error of the model relative to the experimental data and to obtain the noise characteristics of the skid steer mobile robot. Using frequency analysis tools, the noise characteristics are determined and the results of this research is presented and discussed.

2-2   Parameters and states

The following parameters are measured and recorded during the experiments using both various sensors on the jackal and the recording of the Optitrack motion capturing system:

The state of the jackal which is of interest consists of body-frame velocities, which are:

- longitudinal velocity $\dot{x}$ *or* v in $[m/s]$

- lateral velocity $\dot{y}$ *or* u in $[m/s])$

Parameter	Symbol	SI-unit
longitudinal acceleration	$\ddot{x}$	$[m/s^2]$
lateral acceleration	$\ddot{y}$	$[m/s^2]$
rotational velocity around the z-axis (yaw rate)	$\dot{\varphi}$	$[rad/s]$
x position	x	$[m]$
y position	y	$[m]$
heading	ω	$[rad]$
wheel rotational velocity right	$\dot{\omega}_r$	$[rad/s]$
wheel rotational velocity left	$\dot{\omega}_l$	$[rad/s]$
time	t	$[s]$
input velocity command of the jackal	cmd_vel	$[m/s]$ and $[rad/s]$

Table 2-1: List of parameters used in this research

- body rotation velocity around the z-axis (yaw rate) $\dot{\omega}$ in $[rad/s]$

The states are in the body-fixed frame and can be determined from the experimental data of the IMU, rotational encoders in the motors of the jackal and from the position information from the Optitrack system.

2-3   Experiment design

To gather sufficient useful data experiments must be designed with the final goal of this research in mind. A few conditions have to be taken into account when designing the experiments. The jackal robot has a maximum speed of 2 [m/s], which is quite fast given the confined space in which the experiment is to be done and it is not necessary to achieve the maximum speed of the jackal. Skidding is to occur during the experiments, so sufficient rotational motion is required. The confined spaces dictates a closed loop path if the experiment is to run for a longer period of time and a longer path is to be traveled. These conditions have to be met in the experiments. The experiments are performed at two different combinations of input velocities to get insight in velocity dependency. The velocity input for the jackal robot is combination of a longitudinal velocity and an angular velocity. Table 2-2 shows the combination of linear and angular velocity for each series of experiments. The values for the rotational velocity inputs are put in in [deg/s], however, as the rotational velocity is usual given in [rad/s], the values are also presented in the unit of [rad/s]. Both values for the input velocity are changed at the same time for path consistency. The jackal is placed in the same spot at the start of each experiment and drives in counter-clockwise circles. The experimental values have been chosen in such a way that jackal drives along the same path (save for inconsistencies due to skidding, which is to be expected) for both input velocities. Naturally, due to the faster input velocity the time which the jackal needs to complete the experiment run is different for both input velocities.

The following experiments are done using the jackal and the Optitrack system:

- Series of experiments in which circles with a constant radius r and constant velocity v

Experiment series	linear velocity [m/s]	angular velocity [rad/s] ([deg/s])
1	0.3	0.3927 (22.5)
2	0.4	0.5236 (30)

Table 2-2: Input velocities of the experiments

are driven by the jackal. These experiments will be done at two different input velocities v1 and v2 in subsequent experiments

From these performed experiments, the useful data for this research is obtained in the series of experiments in which the robot drives in circles with a constant radius and constant velocity. This data will be analysed in this research. The goal of of this research is characterising the coloured noise which occurs due to unmodelled dynamics whilst the jackal is driving. These experiments are designed in such a way that steady-state turning will be achieved, which results in the need for circle shaped trajectories as a change in the input velocity is not wanted is steady-state turning is to occur for a longer period of time.

2-4   Modelling and Analysis

A linear model will be derived as an aid to estimate the colours process noise due to unmodelled dynamics. The data from the experiments will be used together with the aforementioned linear model to derive the coloured process noise. Due to the number of experiments, the data from experiment 1 at input velocity v1 and experiment 11 at input velocity v2 will be used in the figures in the following chapters.

Chapter 3

Experimental setup

This chapter describes the experimental setup which is used to conduct the experiments for this research. The experimental setup consists of two parts, the jackal robot itself and the Optitrack, which is the external optical motion capturing system. Experiments are performed together with a bachelor group which did preliminary research on the measurement noise of the optitrack system and the occurrence of structures noise in the Jackal [3].

3-1   The jackal, a skid steer mobile robot

The main subject of this research is the jackal [4]. The jackal is a type of skid-steer mobile robot (SSMR) produced by Clearpath Robotics intended for commercial and educational use. Skid steering is a form of differential drive in which there a multiple wheels at the left and right side of the vehicle as opposed to a classic differential drive robot which has only one wheel on each side of the robot. The robot is driven by the wheels and can rotate and steer by a difference in rotational velocity of each wheel. In layman's terms, if the left wheel has a higher rotational velocity then the right wheel, the robot turns right and vice versa. Skid steering works in the same manner but due to the fact that there are multiple wheels at each side instead of just one, the robot skids during a turn.

The size and weight measurements of the jackal are listed in table 3-1. For simulation and testing purposes, Clearpath Robotics supplies an accurate virtual model of the jackal in Gazebo, which is a dynamic simulation environment in ROS [5]. ROS stands for Robot Operation System and is an opensource framework which is used to control robots. The jackal also runs on ROS. To describe the model of the jackal in Gazebo, initial settings files called 'urdf' files are used. The provided urdf [6] file of this model describes the physical properties of the jackal of each separate part which are needed for the dynamical simulation. These values are listed in the following table 3-1.

The total inertia around the z-axis of the body and the four wheels together is not given in the urdf file, only the inertia of the body is given. However, the total inertia of the body and the four wheels together is calculated using the following equation:
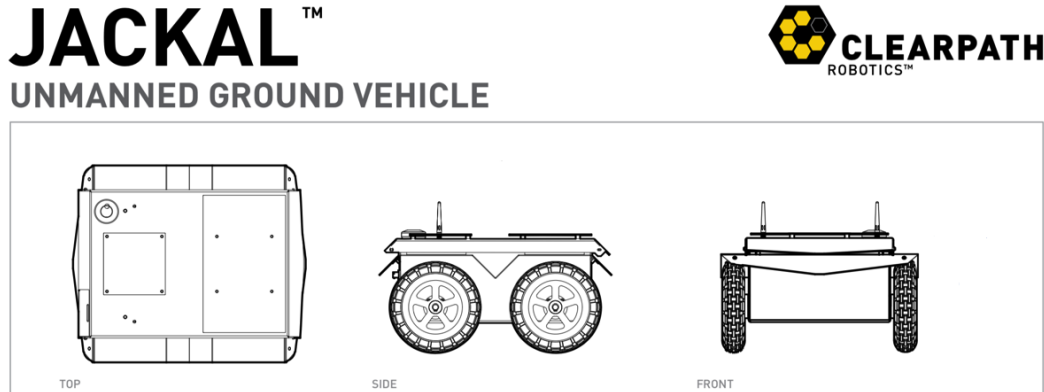
Figure 3-1: Overview of the Jackal by Clearpath robotics [4]

Parameter	Value
length body	0.42 [m]
width body	0.31 [m]
height body	0.184 [m]
wheelbase	0.262 [m]
track width	0.37559 [m]
wheel width	0.04 [m]
wheel radius	0.098 [m]
mass body	16.523 [kg]
mass wheel	0.477 [kg]
inertia body around z-axis	0.4485 $[kg * m^2]$
inertia body + four wheels around z-axis	0.5485 $[kg * m^2]$
a	0.131 [m]
b	0.188 [m]

Table 3-1: Dimensions of the jackal robot as stated by Clearpath Robotics

$$I_{total} = I_{body} + (4 * (m_{wheel} * ((0.5 * wheelbase)^2 + (0.5 * track\ width^2)))) \qquad (3\text{-}1)$$

3-2 The Optitrack, a motion capturing system

To track the movement of the jackal robot via an external observer the Optitrack system located in the Network Embedded Robotics [7] (NERD) lab at DCSC is used. This system consists of 10 infrared camera's which can track objects in 3D-space using reflective markers in a 4 by 9 meter rectangular area at millimetre precision with a maximum frequency of 360 Hz. Figure 3-2 shows the NERDlab:

Figure 3-3 shows the starting orientation of the jackal in the Optitrack, with both the positive x- and y-directions in the body-frame of the jackal and the positive x- and y-directions of the global frame of the Optitrack. The position coordinates of the Optitrack system are recorded
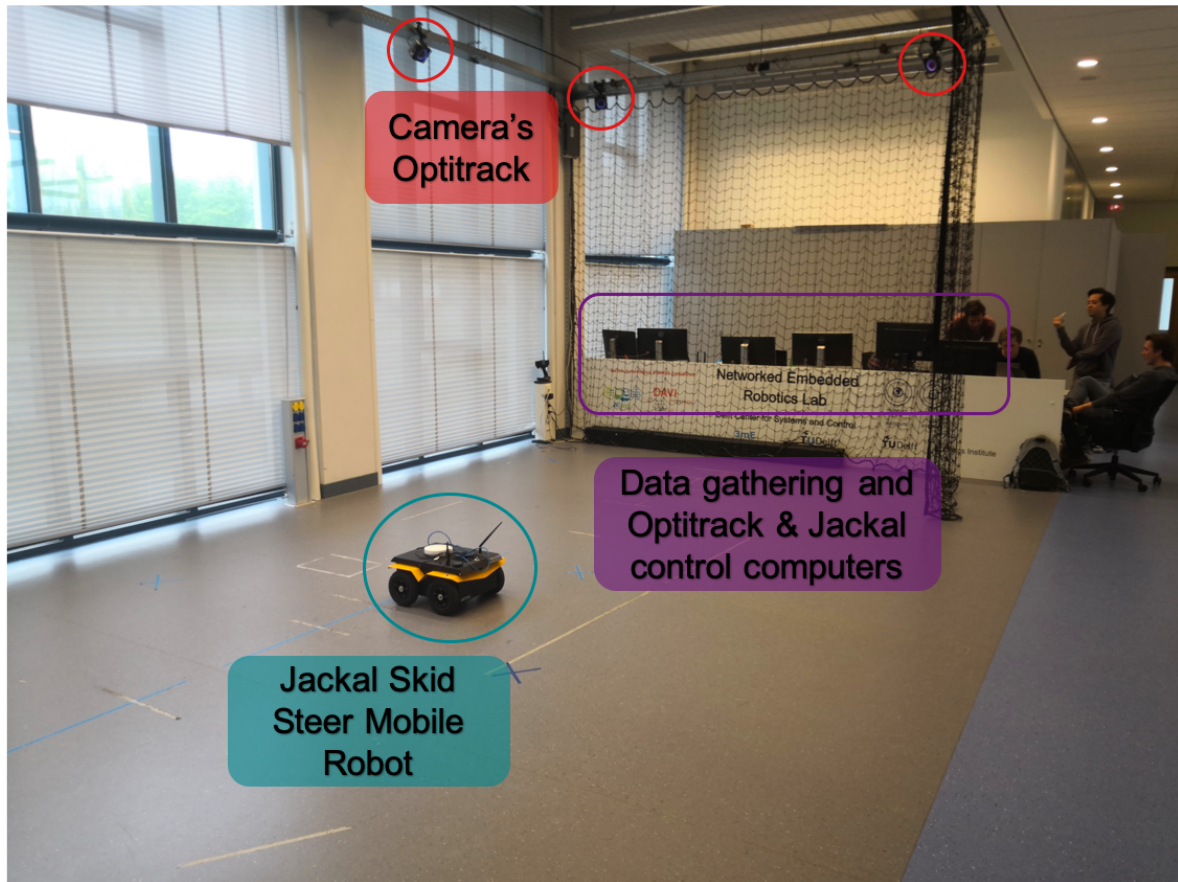
Figure 3-2: NERDlab at DCSC, 3ME, TU Delft [3]

in the global frame, when determining body-frame velocities based on the recorded position information, the body-frame of the jackal has to be rotated to align to the global frame of the Optitrack, which is why the orientation of the global frame is shown in Figure 3-3. Also, to provide a sense of orientation in the space of the NERDlab, the computers are also presented in Figure 3-3.
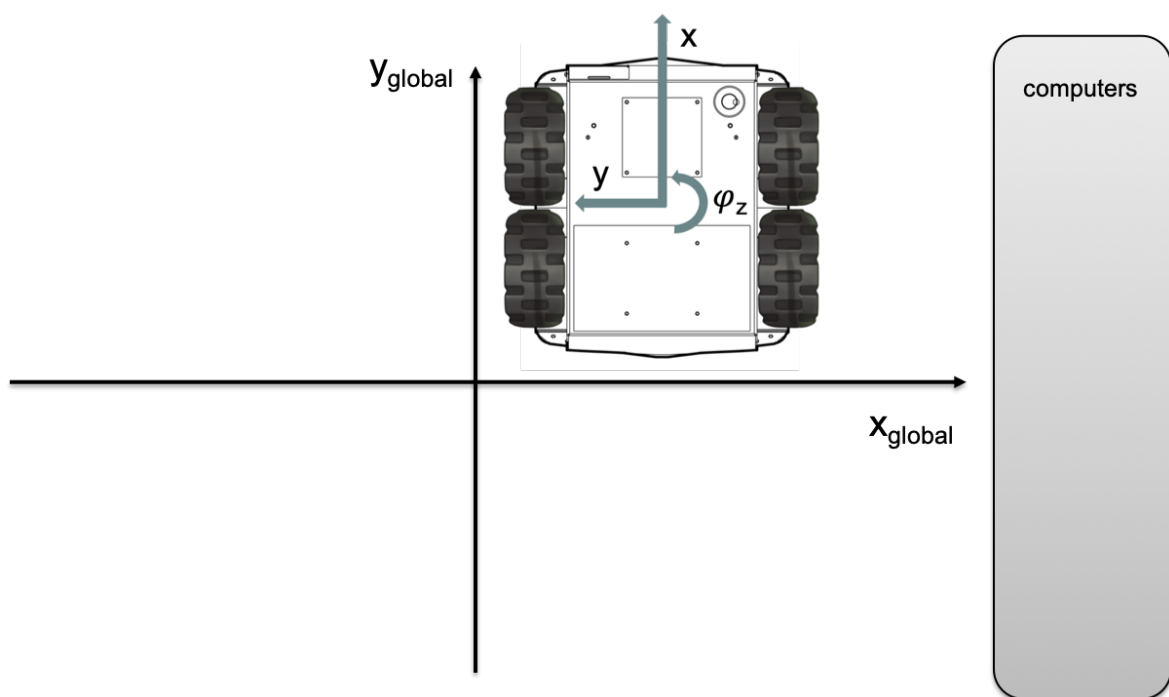
Figure 3-3: Schematic representation of the experiment setup

Chapter 4

Linear dynamical model

The first sub-goal to achieve is the following: *Create a linear dynamical model of the jackal robot and optimize the model in such a way that its velocity states resemble the experimental values of the velocities for the given experimental inputs.* This chapter will elaborate on how that goal is achieved.

4-1 Skid steer vehicle model

As mentioned in previous chapters, the jackal is a skid steer mobile robot which encounters highly non-linear dynamical behaviour when driving due to the skidding nature of the robot. However, the goal is to create a linear dynamical model which is relatively simple and has unmodelled dynamics mainly due to skidding behaviour. To accomplish this a basic model of the skid steer robot has to be developed. This will firstly be done by looking at the existing models in literature and drawing inspiration from those models to create a basic but robust model of the jackal.

4-1-1 Literature

Looking at the literature found as inspiration for the linear model of a skid steer vehicle, the following can be concluded from the works of Wang [8], Yu [9], Wu [10], Zamanian [11]:

- A top-down view of the robot for the free body diagram is prefered because the robot predominantly moves in the x-direction, y-direction and rotation about the z-axis is the way the robot turns.

- Linearisation is very common, skidding is highly non-linear behaviour that is dependent on a lot of factors and very hard to model exactly

- A body-frame perspective on model is useful

- A friction model models the interaction at the contact-point of the wheel and surface

- Kinematic models are also common when describing the skid steer robot but not precise due to skidding

- States of the model are defined as longitudinal, lateral and body rotational velocity

- The input of the model is the wheel rotational velocity

Using this list as a reference, a linear dynamical model can be made of the jackal.

4-1-2 Free body diagram and equations of motion

The first thing that must be done is the creation of the free body diagram of the jackal. This can be seen in Figure 4-1, in which the forces are defined as upwards and to left positive and the moments are defined as left-rotating positive moment, a common approach to defining positive forces and moments. Furthermore, a is defined as the half of the wheelbase of the jackal and b is defined as the half of the track width of the jackal.
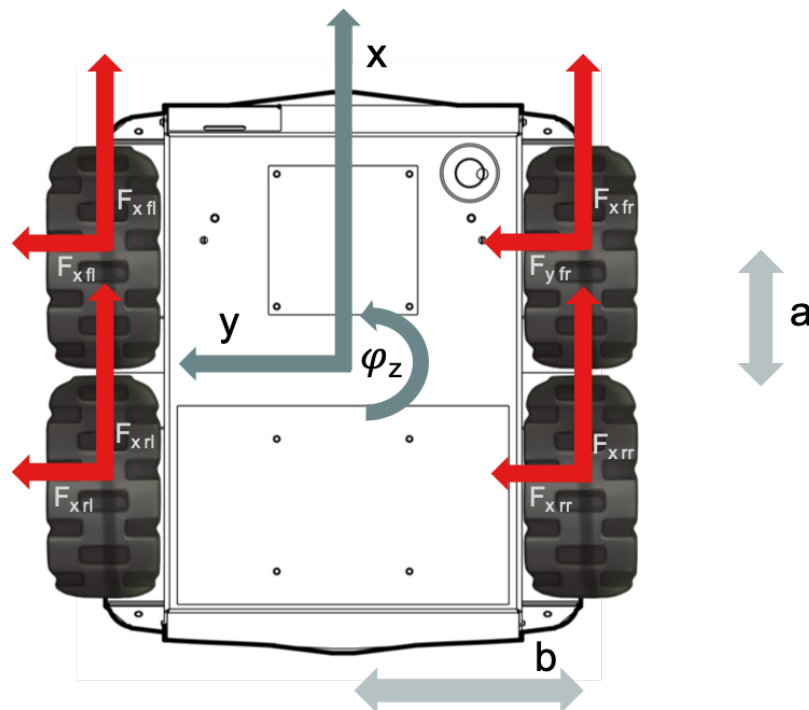
Figure 4-1: Free body diagram of the jackal

Using this free body diagram, the equations of motions are defined as follows:

$$m\ddot{x} = F_{xfr} + F_{xfl} + F_{xrr} + F_{xrl} \tag{4-1}$$

$$m\ddot{y} = F_{yfr} + F_{yfl} + F_{yrr} + F_{yrl} \tag{4-2}$$

$$I\ddot{\varphi} = M_{xfr} + M_{xfl} + M_{xrr} + M_{xrl} + M_{yfr} + M_{yfl} + M_{yrr} + M_{yrl} \tag{4-3}$$

As seen in the free body diagram the points where the forces apply are in the middle of the wheel, as seen from above. The forces in the wheel are the main part of this linear model, the are modeled as linear and in a relatively basic but robust way. Both the longitudinal and lateral contact forces are defined as a viscous damping force. The longitudinal force can be seen in the following equations, with $i = front\ or\ rear$ and $j = right\ or\ left$ and it incorporates both the forward velocity of the body and the wheel rotational velocity which drives the robot:

$$F_{xij} = -d_{long}u \tag{4-4}$$

$$u = u_{axle} + u_{rotation} \tag{4-5}$$

$$u_{rotation} = -\omega_j \cdot r_{wheel} \tag{4-6}$$

$$u_{axle} = \dot{x} + b\dot{\varphi} \tag{4-7}$$

The lateral force in each wheel is defined as a viscous damping force int the following way, with $i = front\ or\ rear$ and $j = right\ or\ left$, which only incorporates the sideways velocity of the body as the wheels cannot rotate in the y-direction:

$$F_{yij} = -d_{lat}v \tag{4-8}$$

$$v = v_{axle} \tag{4-9}$$

$$v_{axle} = \dot{y} + a\dot{\varphi} \tag{4-10}$$

Filling in the equations for all eight forces results in the following equations:

$$F_{xfr} = -d_{long}\dot{x} - d_{long}b\dot{\varphi} + d_{long}r_{wheel}\omega_r \tag{4-11}$$

$$F_{xfl} = -d_{long}\dot{x} + d_{long}b\dot{\varphi} + d_{long}r_{wheel}\omega_r \tag{4-12}$$

$$F_{xrr} = -d_{long}\dot{x} - d_{long}b\dot{\varphi} + d_{long}r_{wheel}\omega_r \tag{4-13}$$

$$F_{xrl} = -d_{long}\dot{x} + d_{long}b\dot{\varphi} + d_{long}r_{wheel}\omega_r \tag{4-14}$$

$$F_{yfr} = -d_{lat}\dot{y} + d_{lat}a\dot{\varphi} \tag{4-15}$$

$$F_{yfl} = -d_{lat}\dot{y} + d_{lat}a\dot{\varphi} \tag{4-16}$$

$$F_{yrr} = -d_{lat}\dot{y} - d_{lat}a\dot{\varphi} \tag{4-17}$$

$$F_{yrl} = -d_{lat}\dot{y} - d_{lat}a\dot{\varphi} \tag{4-18}$$

The moments are defined as follows using the previously defined forces and the parameters a and b:

$$M_{xij} = bF_{xij} \tag{4-19}$$

$$M_{yij} = aF_{yij} \tag{4-20}$$

Filling in the equations for the eight moments results in the following equations for all eight moments:

$$(-)M_{xfr} = bF_{xfr} = -d_{long}b\dot{x} - d_{long}b^2\dot{\varphi} + d_{long}br_{wheel}\omega_r \tag{4-21}$$

$$(+)M_{xfl} = bF_{xfl} = +d_{long}b\dot{x} - d_{long}b^2\dot{\varphi} - d_{long}br_{wheel}\omega_l \tag{4-22}$$

$$(-)M_{xrr} = bF_{xrr} = -d_{long}b\dot{x} - d_{long}b^2\dot{\varphi} + d_{long}br_{wheel}\omega_r \tag{4-23}$$

$$(+)M_{xrl} = bF_{xrl} = +d_{long}b\dot{x} - d_{long}b^2\dot{\varphi} - d_{long}br_{wheel}\omega_l \tag{4-24}$$

$$(-)M_{yfr} = aF_{yfr} = -d_{lat}a\dot{y} - d_{lat}a^2\dot{\varphi} \tag{4-25}$$

$$(-)M_{yfl} = aF_{yfl} = -d_{lat}a\dot{y} - d_{lat}a^2\dot{\varphi} \tag{4-26}$$

$$(+)M_{yrr} = aF_{yrr} = +d_{lat}a\dot{y} - d_{lat}a^2\dot{\varphi} \tag{4-27}$$

$$(+)M_{yrl} = aF_{yrl} = +d_{lat}a\dot{y} - d_{lat}a^2\dot{\varphi} \tag{4-28}$$

When combining the previous forces and moments into equations 4-1 you get the following equations of motion:

$$\ddot{x} = \frac{-4d_{long}}{m}\dot{x} + \frac{2d_{long}r_{wheel}}{m}\omega_r + \frac{2d_{long}r_{wheel}}{m}\omega_l \tag{4-29}$$

$$\ddot{y} = \frac{-4d_{lat}}{m}\dot{y} \tag{4-30}$$

$$\ddot{\varphi} = \frac{-4}{I}(b^2d_{long} + a^2d_{lat}) + \frac{2bd_{long}r_{wheel}}{I}\omega_r - \frac{2bd_{long}r_{wheel}}{I}\omega_l \tag{4-31}$$

In state-space formulation these equations of motions are, with the noise which has to be proven added as w:

$$\begin{pmatrix} \ddot{x} \\ \ddot{y} \\ \ddot{\varphi} \end{pmatrix} = \begin{pmatrix} \frac{-4d_{long}}{m} & 0 & 0 \\ 0 & \frac{-4d_{lat}}{m} & 0 \\ 0 & 0 & \frac{-4}{I}(b^2d_{long} + a^2d_{lat}) \end{pmatrix} \begin{pmatrix} \dot{x} \\ \dot{y} \\ \dot{\varphi} \end{pmatrix} + \begin{pmatrix} \frac{2d_{long}r_{wheel}}{m} & \frac{2d_{long}r_{wheel}}{m} \\ 0 & 0 \\ \frac{2bd_{long}r_{wheel}}{I} & -\frac{2bd_{long}r_{wheel}}{I} \end{pmatrix} \begin{pmatrix} \omega_r \\ \omega_l \end{pmatrix} + w \tag{4-32}$$

4-1-3   Model inputs and outputs

After defining the state-space formulation of the linear dynamical model of the skid steer robot it is implemented in MATLAB for simulation and analysis purposes. To simulate a motion of the skid steer vehicle, an input has to be given to it in the form of a right and left rotational velocity. However, in the experiments of the real-life jackal, the input velocity of

the jackal is given in $\dot{x}_{input}$ and $\dot{\varphi}_{input}$. This needs to be translated into ω_l and ω_r as inputs for the model and simulation. Looking at the implementation of the jackal model in Gazebo by Clearpath Robotics, it uses the differential drive controller of ROS [12]. This controller computes the rotational velocities for the left and the right wheel in the following way:

$$\omega_l = (0.5 * (\dot{x}_{input} - \dot{\varphi}_{input}))/r_w \tag{4-33}$$

$$\omega_r = (0.5 * (\dot{x}_{input} + \dot{\varphi}_{input}))/r_w \tag{4-34}$$

The outputs of the model is the velocity state of the model, which consists of the longitudinal, lateral and rotational velocity, the exact parameters are listed in the following list:

- $\dot{x}$ - longitudinal velocity [m/s]

- $\dot{y}$ - lateral velocity [m/s]

- $\dot{\varphi}$ - rotational velocity [rad/s]

The next step is to find a value for d_{lat} and d_{long} which results in a simulated velocity which matches the experimental values for the velocity states measured in the experiments. This will be done in the next chapter.

Optimisation of the linear dynamical model

To ensure that the simulation behaves like a real skid steer vehicle, the outputs of the simulation are compared to the experimental results of the jackal. The real input used in the experiments is used as input on the simulation of the jackal. Looking at the way the forces are defined, there is room to tune the model using the damping coefficients d_{lat} and d_{long}, in such a way that the output of the model matches the experimental results as close as possible. How this is done is explained in this chapter.

5-1 Theoretical range of longitudinal and lateral damping coefficient values

To optimise d_{lat} and d_{long}, knowledge is needed on the range of realistic damping-coefficients for rubber tyres on surfaces. From literature this range is determined to be $100-1000 \ kg/s \ or \ Ns/m$ for rubber pneumatic tyres, which are the tyres that the jackal has. This range is determined from reviewing tyre damping coefficients used in the lumped Lugre friction model [13] and [14] which uses values in the range of 150 Ns/m to 500 Ns/m, and in the magic formula of Pacejka as implemented in MATLAB [15] which uses a value of 1000 Ns/m for the tyre damping coefficient used in the tyre model in MATLAB. However, taking into account that these papers and formula's are used to model real-life car tyres, the smaller size of the jackal and the smaller tyres of the jackal in comparison to a typical car might mean that the most efficient dampingscoefficient lies in a lower range than stated in literature. For this reason, the range will be extended at the lower bound towards a lower value of 10. The total range which will be used in the optimisation will be $10-1000 \ kg/s \ or \ Ns/m$.

5-2 Optimisation method

To determine the optimal value for both d_{lat} and d_{long}, two vectors are created containing all possible values for d_{lat} and d_{long} in the range of $10 - 1000$ kg/s or Ns/m. When doing this in increments of whole numbers, the total number of simulations that would be done is $1000 * 1000 * 2 = 2000000$, as 1000 values lie in the range of $10 - 1000$ when taking incremental steps of 1 and the simulations are done for both the input velocities v1 and v2. Each simulation takes around one second to complete. This would result in an estimated simulation time of 555 hours, or almost 23 full days using the computational power readily available for this research. It is clear that this will cost too much time for such an optimisation. As the linear model is already a very rough approximation of reality, the range of values which will be evaluated is divided into increments of 10, starting at 10 and ending at 1000. This will lead to an acceptable simulation time of approximately 5.5 hours to compute all possible solutions at both input velocities.

For all these simulations, the velocity state of the simulated jackal model is saved at each timestep in order to compare the values of these simulated velocities against the experimental values of the velocity state of the jackal. However, the sensors equipped in the experimental setup are not able the accurately and directly measure the entire velocity state $\dot{x}, \dot{y}, \dot{\varphi}$ of the jackal. The motion capturing system is able to directly determine and measure the position and heading x, y, φ of the jackal and the internal IMU is able to measure $\ddot{x}, \ddot{y}, \dot{\varphi}$ of the jackal. That means that the only part of the velocity state which is directly measured and not inferred during the experiments is $\dot{\varphi}$, the rotational velocity of the jackal. Due to $\dot{\varphi}$ being the only directly measurable part of the velocity state, d_{lat} and d_{long} will have values which will correspond to a minimal error between the simulated and experimental values of $\dot{\varphi}$.

The error between the simulated and experimental values for $\dot{\varphi}$ is calculated using the mean squared error (MSE). The mean squared error is the mean of the sum of the squared difference between the simulated and experimental values at each timestep, as stated in the next equation. This is calculated for each simulated pair of d_{lat} and d_{long} in the range of $100 - 1000$ kg/s.

$$MSE = \frac{1}{n}\Sigma_{i=1}^{n}\left(\dot{\varphi}_{sim_i} - \dot{\varphi}_{exp_i}\right)^2 \tag{5-1}$$

The experiments were done at two different input velocities v_1 & v_2, with ten experiments being done at v_1 and five experiments being done at v_2. For each input velocity, the mean of the MSE (MMSE) is calculated by summing the MSE for each pair of d_{lat} and d_{long} for each experiment and dividing by the number of experiments. This yields a mean of the MSE for each pair of d_{lat} and d_{long}, as can be seen in the following equation with k = number of experiments.

$$mean\ of\ MSE = \frac{1}{k}\Sigma_{i=1}^{k}MSE_k \tag{5-2}$$

This is a measure for the error between the simulated and experimental values of $\dot{\varphi}$. The pair of values for d_{lat} and d_{long} which yield a minimal value of $\dot{\varphi}$ is then chosen as the optimal pair of values for d_{lat} and d_{long}. The errors for all possible pairs of d_{lat} and d_{long} are plotted against d_{lat} and d_{long} to gain an insightful graphical representation.

5-2-1   Results

The values of the damping coefficients for which the MSE is the smallest are obtained and for v1 are:

- $d_{lat} = 110 \ Ns/m$

- $d_{long} = 30 \ Ns/m$

- $error = 0.0467 \ rad/s$

The mapping of the MSE versus d_{lat} and d_{long} for input velocity v1 can be seen in Figure 5-1.
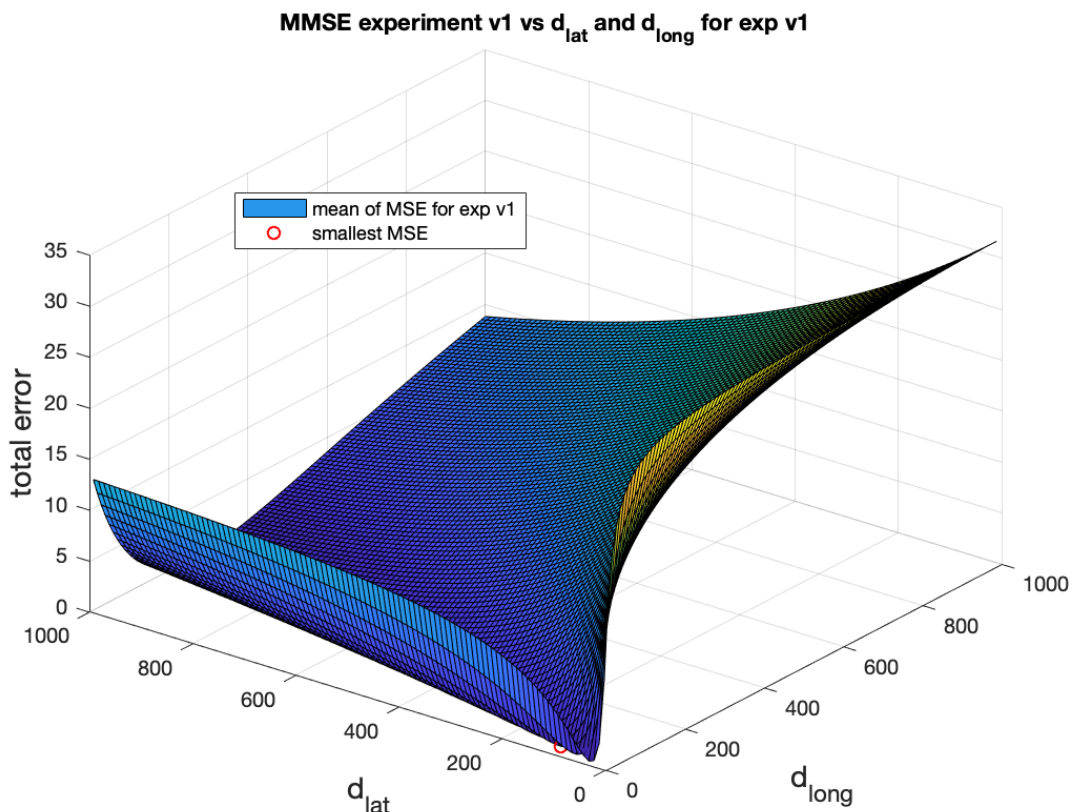
Figure 5-1: Mapping of the MSE versus the possible set of longitudinal and lateral damping coefficients for input velocity v1

For the faster experiment at v2 the values are listed below and the mapping of the MSE versus d_{lat} and d_{long} for input velocity v2 can be seen in Figure 5-2.

- $d_{lat} = 110 \ Ns/m$

- $d_{long} = 30 \ Ns/m$

- $error = 0.0073 \ rad/s$
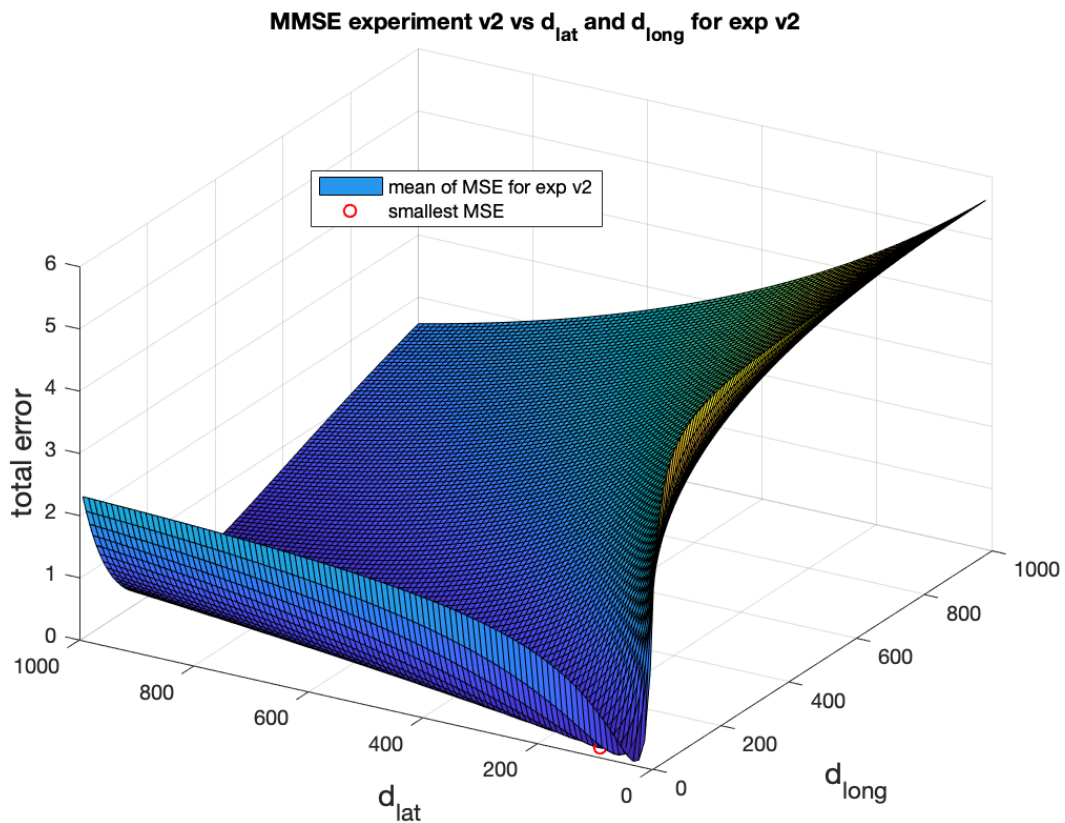
Figure 5-2: Mapping of the MSE versus the possible set of longitudinal and lateral damping coefficients for input velocity v2

The values above shows that for a different input velocity, the optimal parameter for d_{lat} and d_{long} are the same. However as this optimisation is looking for an optimal value for d_{lat} and d_{long} for both experiments, both means of MSE ($MMSE_{v1}$ and $MMSE_{v2}$) added together to create the total MMSE $MMSE_{total}$.

$$MMSE_{total} = MMSE_{v1} + MMSE_{v2} \tag{5-3}$$

This is done in order to ensure that the local optimal values for d_{lat} and d_{long} for experiments done with velocity v1 and v2 are actually not only local optimal values at each input velocity but also global optimal values. It might be possible that $MMSE_{total}$ for another pair d_{lat} and d_{long} is actually smaller than smallest local $MMSE_{v1}$ and $MMSE_{v2}$ for that specific pair of

d_{lat} and d_{long}. It is not likely though as the values of d_{lat} and d_{long} which yield the smallest MMSE are the same for the experiments at both velocities. The values for d_{lat} and d_{long} which yield the smallest $MMSE_{total}$ are listed below and the mapping of the MSE versus d_{lat} and d_{long} for both input velocities v1 and v2 can be seen in Figure 5-3.

- $d_{lat} = 110 \ Ns/m$

- $d_{long} = 30 \ Ns/m$

- $error = 0.0510 \ rad/s$
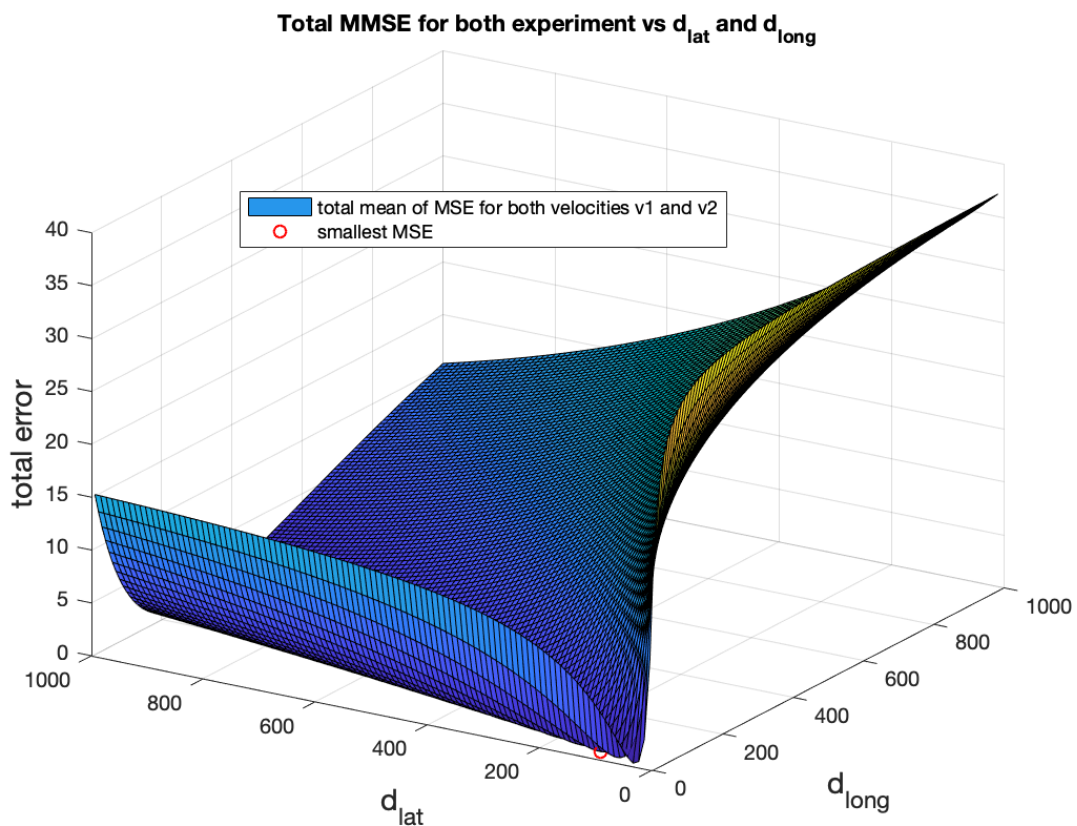
Figure 5-3: Mapping of the MSE versus the possible set of longitudinal and lateral damping coefficients for input velocity v1 and v2

These values are exactly the same as the values of d_{lat} and d_{long} for $MMSE_{v1}$ and $MMSE_{v2}$ and are then chosen as the values for the d_{lat} and d_{long} which are used in this model.

5-2-2 Remarks

Another interesting observation can be made. Looking at Figure 5-4 which depicts the mapping of d_{lat} and d_{long} in a top-down view, a larger group of values for both d_{lat} and d_{long} can

be found which also have a acceptable small error. Looking into these values for d_{lat} and d_{long}, the common denominator is that the value for d_{lat} is $3\frac{2}{3}$ times larger then the value of d_{long}. A line can be drawn which is the representation of the linear equation $y = 3\frac{2}{3}x$ over these points. All combinations of d_{lat} and d_{long} along this line will lead to an acceptable mean squared error of $0.0691[rad/s]$ for $d_{lat} = 990$ and $d_{long} = 270$. This error is $\frac{(0.0691 - 0.0510)}{0.0510} = 36\%$ larger than the smallest error found in the previous chapter. When deviating from this line the mean squared error instantly increases with much higher percentages.
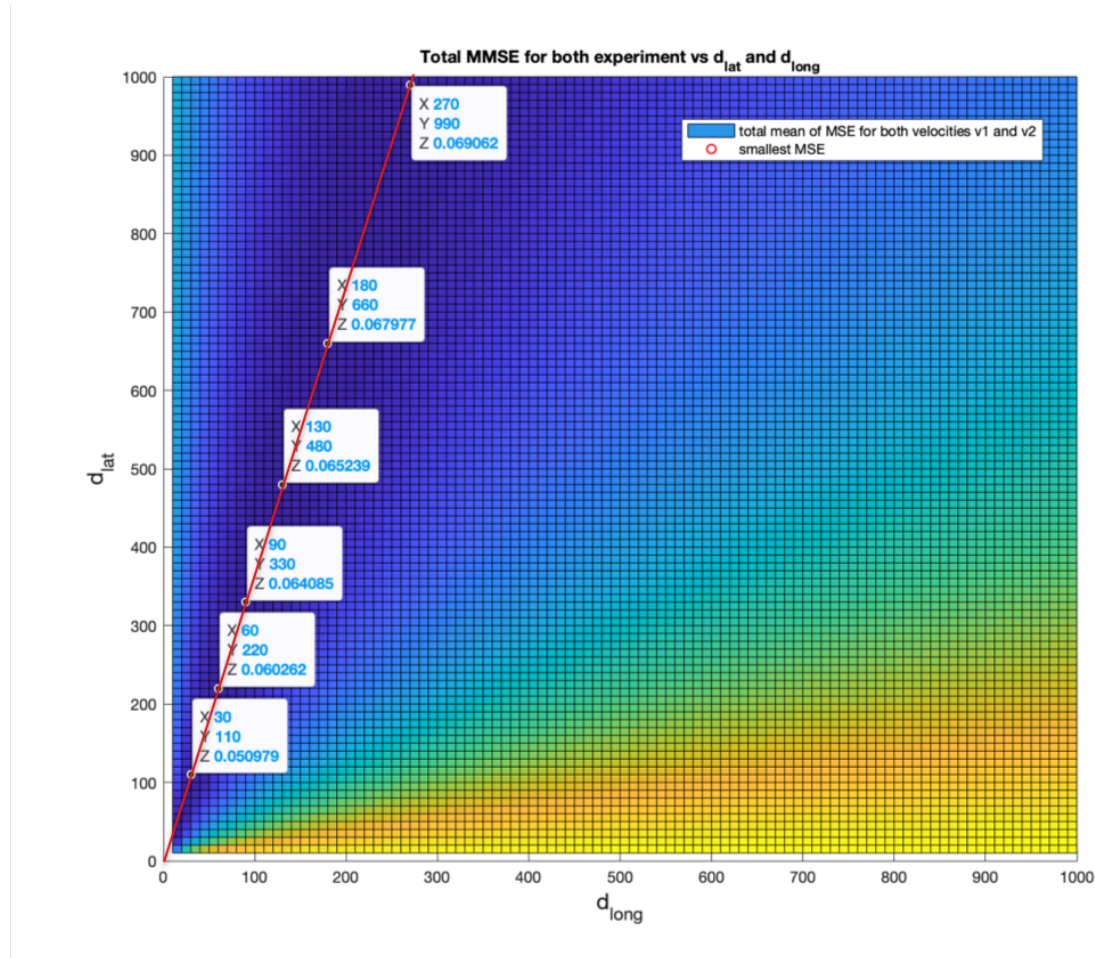
Figure 5-4

5-2-3   Checking the optimised values

The rotational velocity of the simulation can be seen plotted on top of the first experiment at input velocity v1 in Figure 5-5 and plotted on top the first experiment at input velocity v2 in Figure 5-6 which illustrates a small error in the model for the rotational velocity. Which then shows that as far as the rotational velocity goes, the model is fairly accurate, the values for the simulation lie in the range of real world values found in the experiments.
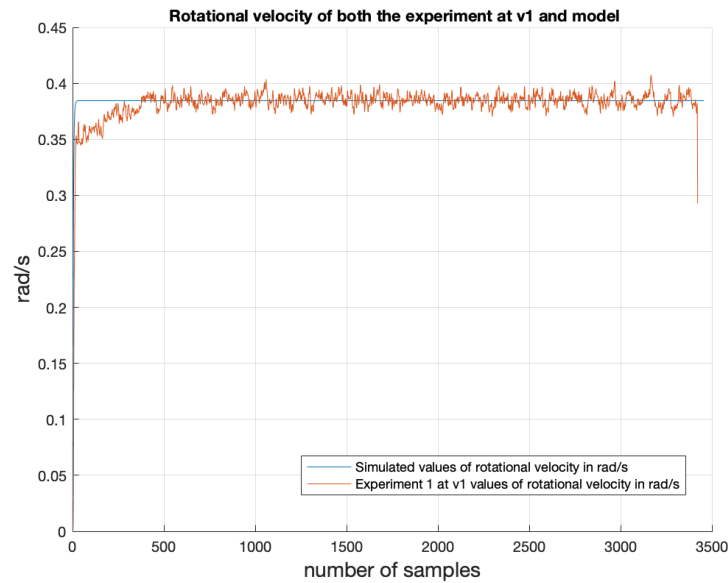
Figure 5-5: The rotational velocity $\dot{\varphi}$ of both the model of the jackal robot and the experimental values of the jackal for the first experiment done at input velocity v1
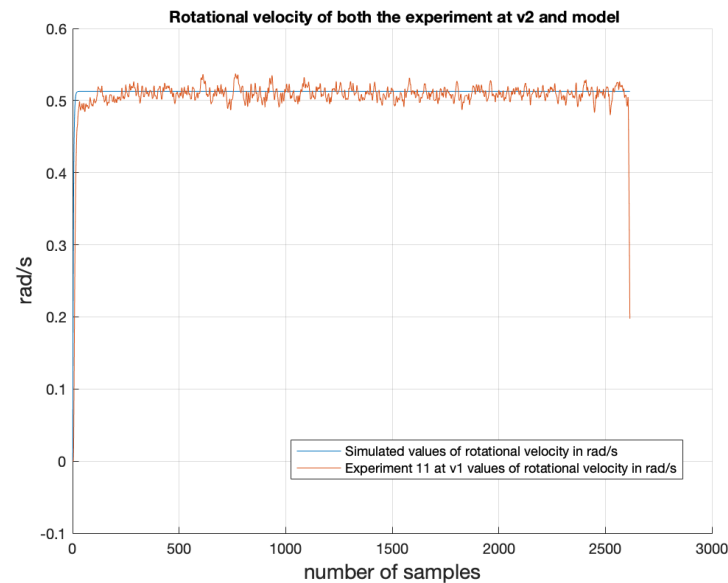
Figure 5-6: The rotational velocity $\dot{\varphi}$ of both the model of the jackal robot and the experimental values of the jackal for the first experiment done at input velocity v2

5-3 Obtaining $\dot{x}$ and $\dot{y}$

The longitudinal velocity $\dot{x}$ and lateral velocity $\dot{y}$ cannot be measured directly by the experimental setup as the IMU measures accelerations and rotational velocities and the motion capturing system measures positions and heading of the jackal. The encoders present in the

motors of the jackal measure the rotational velocity of the wheels on the left and the wheels on the right. In theory, the rotational velocity of the wheel has a direct relation to the longitudinal velocity of the vehicle as the longitudinal velocity of a wheel due to the rotational velocity is expressed as: $\dot{x} = \omega_{wheel} * r_{wheel}$. The rotational velocities for the left and the right wheel in experiments with input velocities v1 and v2 are shown in Figures 5-7 and 5-8. It is clear that the robot turns in a counter clockwise fashion as the rotational velocity of the right wheels is higher than the rotational velocity of the left wheels. It is also interesting to see that there is a certain pattern in the rotational velocity of both the left and the right wheels which coincides. This might be due to the fact that the surface on which the jackal was driving was stickered in certain places during the experiment. These stickered area's have different surface properties which might result in more or less skidding of the jackal. Which in turn results in a higher or lower rotational velocity of the wheels.
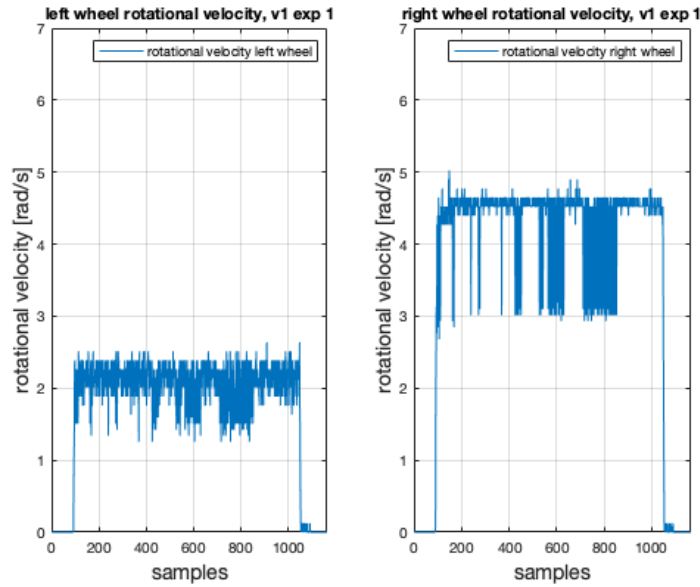
Figure 5-7: The rotational velocity of the left and the right wheel of the jackal robot for experiment 1 at input velocity v1

Using and substituting equations (4-33) and (4-34) used in chapter 4 to calculate the rotational velocities of each wheel, the following equation is derived to calculate the longitudinal velocity from the rotational velocities of each wheel.

$$\dot{x} = r_w * (\omega_l + \omega_r) \tag{5-4}$$

This leads to the longitudinal velocity of the jackal when there is zero slip and all the rotational velocity is translated into longitudinal velocity. In this case however, there is a lot of slip present, this means that the wheels will rotate faster or slower than expected and the data from the encoders cannot be used to calculate the longitudinal velocity of the jackal. This is verified using the experimental data from the encoder. When recalculating the rotational velocity of the wheels into the longitudinal velocity of the jackal more than twice as
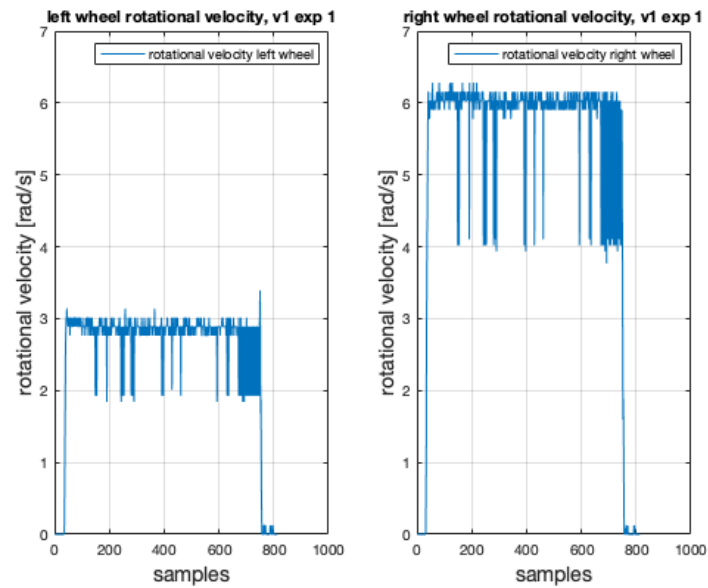
Figure 5-8: The rotational velocity of the left and the right wheel of the jackal robot for experiment 11 at input velocity v2

high longitudinal velocities are found then the longitudinal velocity given in the control script of the jackal. The results for the recalculated velocities from the experimental data of the encoders for experiment 1 at input velocity v1 are shown in Figure 5-9.
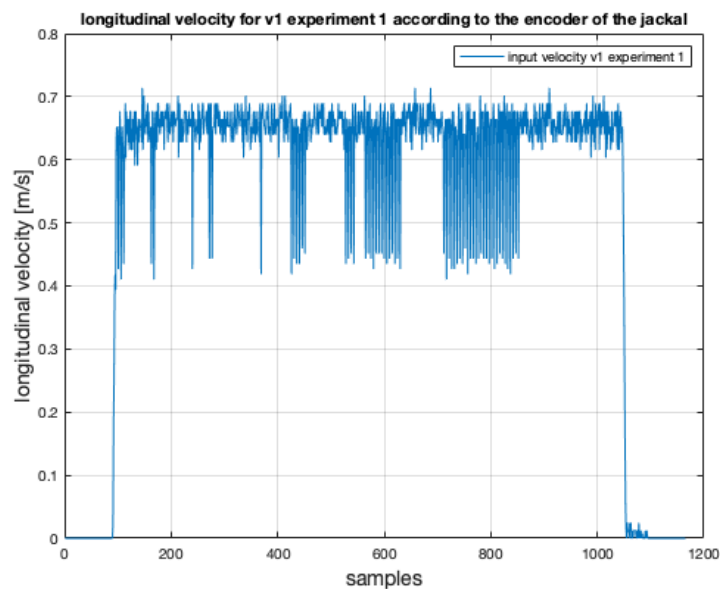
Figure 5-9: Longitudinal velocity $\dot{x}$ of the jackal in experiment 1 at input velocity v1 when using the experimental encoder data to reconstruct the longitudinal velocity
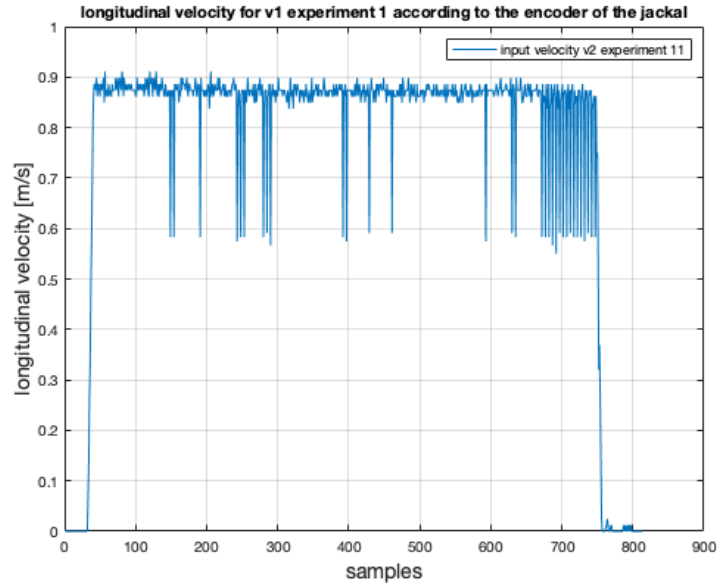
Figure 5-10: Longitudinal velocity $\dot{x}$ of the jackal in experiment 11 at input velocity v2 when using the experimental encoder data to reconstruct the longitudinal velocity

As can be seen in Figure 5-9, the longitudinal velocity when calculated from the rotational velocity measured by the encoders is much higher, with a mean velocity of 0.53 [m/s] and a median velocity of 0.65 [m/s], than the longitudinal input velocity of 0.3 [m/s]. This is both not true and not possible as the expected velocity of the jackal cannot be higher than the input velocity the jackal receives. The same behaviour can be seen in 5-10 which shows the calculated longitudinal velocity based on the encoders for experiment number 11 which uses the faster velocity input v2. Again, the mean of the calculated longitudinal velocity is 0.76 [m/s] and a median velocity of 0.87 [m/s], which is much higher than the longitudinal input velocity of 0.4 [m/s]. Such a high deviation is very strange behaviour. Skidding of the jackal is not expected to have such a high effect on longitudinal velocity that the wheels are actually rotating more than twice as fast as expected with regard to the input velocity. This shows that using the encoders to estimate the longitudinal velocity is not useful.

Having concluded that the encoders cannot be used to obtain the longitudinal velocity for these experiments, the following approach is considered. It is possible to obtain the longitudinal and lateral velocity using either the IMU or the motion capturing system. The IMU is already in the body-fixed frame and the values for the acceleration have to be integrated the obtain the longitudinal and lateral velocities of the jackal.

The data from the motion capturing system can also be used to obtain the longitudinal and lateral velocity. The positions and heading of the jackal are in the global frame of the motion capturing system and thus have to be converted to the body-fixed frame and the values have to differentiated to obtain the velocities from the body-fixed positions.

However, integrating the accelerations measured in the IMU yields an acceleration drift which does not occur in differentiating the position of the jackal. This drift might be compensated using the differentiated velocities but for now the differentiated velocities, however spikey and not perfectly accurate, are used to estimate the longitudinal and lateral velocities $\dot{x}$ and $\dot{y}$.

An example of the longitudinal and lateral velocity calculated from the position and heading data of the motion capturing system can be seen in Figure 5-11 and Figure 5-12. In these figures, the longitudinal and lateral velocities for experiment 1 at input velocity v1 are shown.
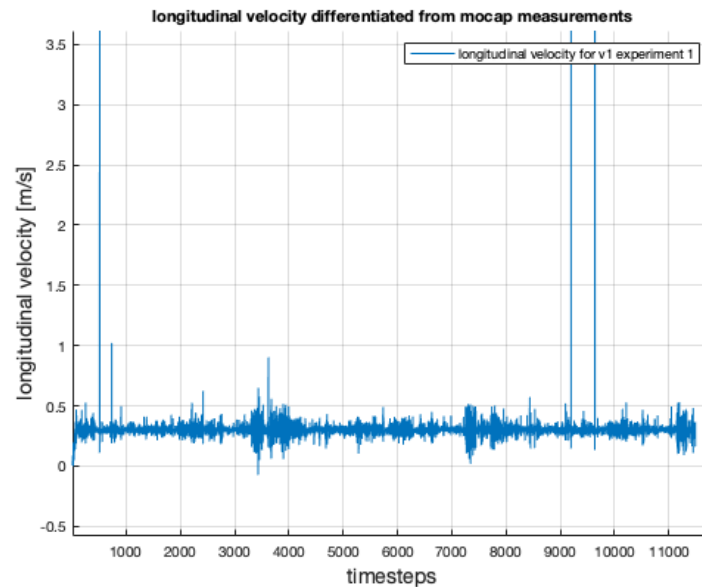
Figure 5-11: Longitudinal velocity of the jackal inferred using data obtained by the motion capturing system for experiment 1 at input velocity v1
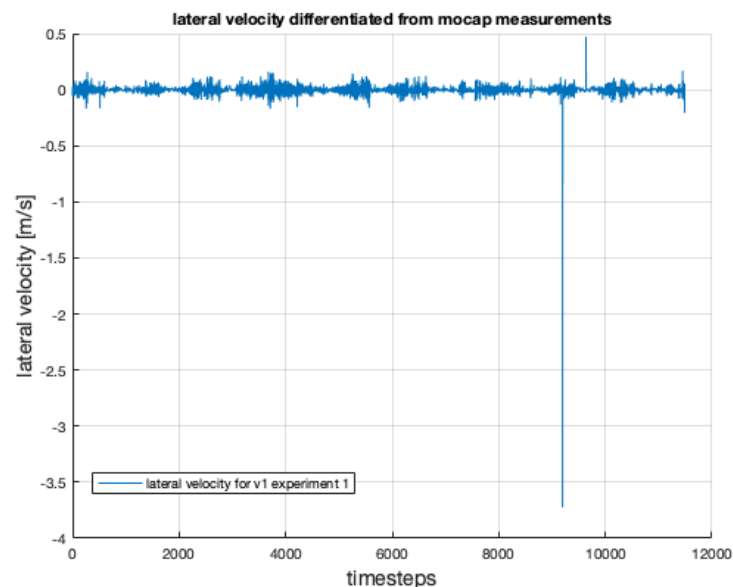
Figure 5-12: Lateral velocity of the jackal inferred using data obtained by the motion capturing system for experiment 1 at input velocity v1

Comparing the longitudinal and lateral velocities measured during the experiments to the

optimised model,the following Figures 5-13, 5-14, 5-15 & 5-16 show the simulation output for $\dot{x}$ and $\dot{y}$ plotted on top of the experimental values of $\dot{x}$ and $\dot{y}$ for both input velocities v1 and v2.
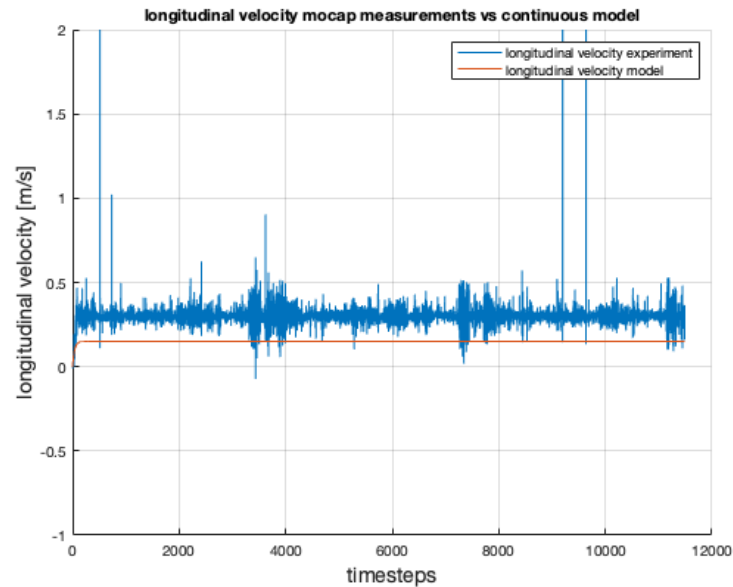
Figure 5-13: The longitudinal velocity $\dot{x}$ of both the model of the jackal robot and the experimental values of the jackal for the first experiment done at input velocity v1, inferred using data obtained by the motion capturing system
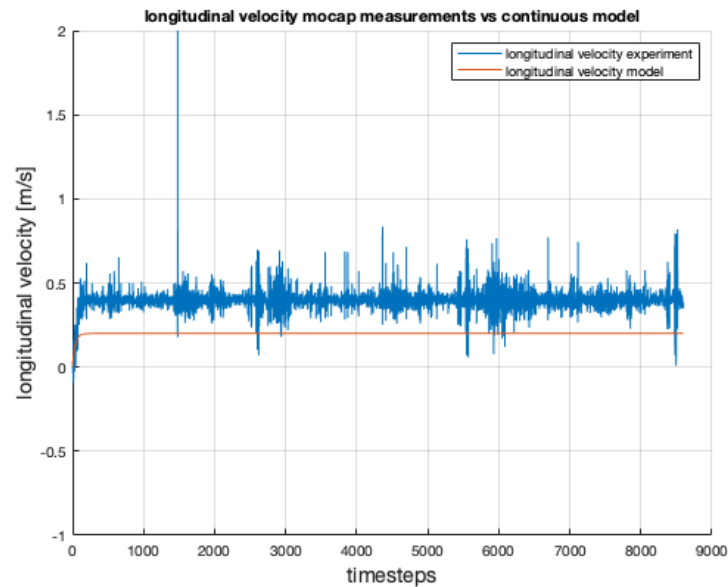
Figure 5-14: The longitudinal velocity $\dot{x}$ of both the model of the jackal robot and the experimental values of the jackal for the first experiment done at input velocity v2, inferred using data obtained by the motion capturing system
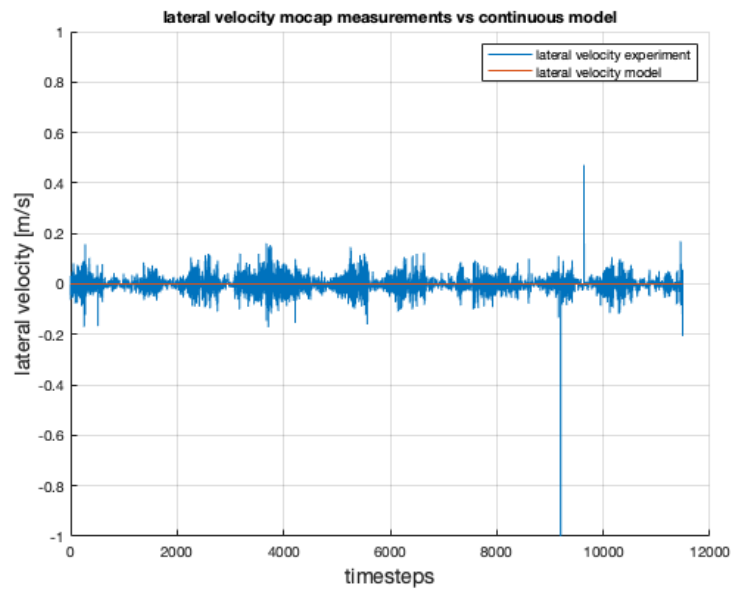
Figure 5-15: The lateral velocity $\dot{y}$ of both the model of the jackal robot and the experimental values of the jackal for the first experiment done at input velocity v1
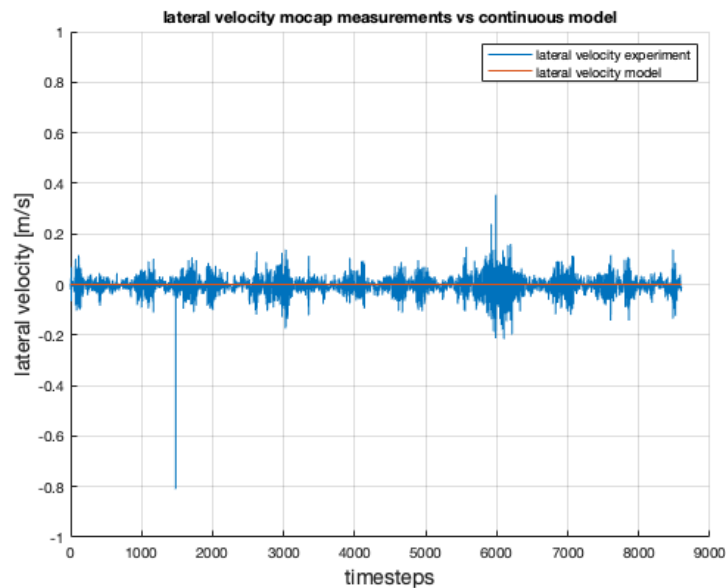
Figure 5-16: The lateral velocity $\dot{y}$ of both the model of the jackal robot and the experimental values of the jackal for the first experiment done at input velocity v2

The model is now tuned to ensure behaviour which closely resembles the velocity behaviour of the jackal robot during the experiments. It is however not perfect, especially with respect to the longitudinal and lateral velocity of the model versus the experimental values. But it is believed that the error for those velocities not only stems from a model discrepancy as the model is tuned to reflect the rotational velocity optimally but also stems from the fact that

the longitudinal and lateral velocity are not directly measured during the experiment. The differentiation of the position data introduces extra noise and this can be seen in Figures 5-11 and 5-12. The next step is to discretise the tuned linear dynamical model to get a prediction for the state for each next step k+1. This is done in the next chapter.

Chapter 6

Discretisation

This chapter will elaborate on the steps which have to be taken to prove that the jackal actually suffers from coloured noise, which will be proven in chapter seven. In chapters four and five, both the linear model of the jackal and the error between the measured experimental values and the simulated values of the model have been described. But this error is not actually the coloured noise which the jackals suffers from. The noise the jackal suffers from is actually the difference between the prediction made by the model of the state of the jackal for the next step in time and the actually measured experimental value of that next step in time. This chapter describes the discretisation method needed for transforming the continuous time model described in the previous chapters into a discrete time model.

6-1   Next step state prediction

The following part elaborates on the discretisation of the linear dynamical model of the jackal. The discretised system predicts the state of the model at the next step based on the input at step k and the state at step k. This is done to get an estimate for each next step $[k+1]$ of the state of the jackal. The error for each prediction is needed as this will yield the noise for each next state $[k+1]$ when comparing the experimental values of state $[k+1_{exp}]$ and the estimated values of $[k+1_{est}]$ when the experimental values of $[k_{exp}]$ are fed into the discretised linear dynamical system to get an estimate of the values of state $[k+1_{est}]$.

6-2   Discretising vehicle model

In chapter four the state space equations for the continuous system is presented. These state space equations have to be discretised to obtain the discrete time state space equations of the linear dynamical system. The set of continuous state space equations will be in the following general form:

$$\dot{\mathbf{x}} = A\mathbf{x}(t) + Bu(t) + w(t) \tag{6-1}$$

In which the state $\mathbf{x}$:

$$\mathbf{x} = \begin{pmatrix} \dot{x} \\ \dot{y} \\ \dot{\varphi} \end{pmatrix} \tag{6-2}$$

and the state $\dot{\mathbf{x}}$

$$\dot{\mathbf{x}} = \begin{pmatrix} \ddot{x} \\ \ddot{y} \\ \ddot{\varphi} \end{pmatrix} \tag{6-3}$$

Which converts to the following set of discrete state space equations with $\hat{A}$ and $\hat{B}$ representing the discretised matrices A and B in the continuous state space equation form:

$$x[k+1] = \hat{A}x[k] + \hat{B}u[k] + w[k] \tag{6-4}$$

To discretise the continuous system two different methods are researched and tested. The first method is the Euler method of discretisation (which is an approximation):

$$x[k+1] = x[k] + Ax[k]dT + Bu[k]dT + w[k] \tag{6-5}$$

The second method is the exact method of discretisation, with I being the identity matrix:

$$x[k+1] = e^{AdT}x[k] + A^{-1}(e^{AdT} - I)Bu[k] \tag{6-6}$$

The outputs of the Euler method and the exact method are different when simulation the first few steps of the input, so further investigation was needed, concluding that the timestep $dT = \frac{1}{F_{imu}} = \frac{1}{72}$ which was used to calculate the next prediction of the state is too large to use the Euler method with reasonable output for the acceleration part (first few steps) of the prediction of the velocities. The Euler method is an approximation for the discretisation of a system and not the exact method of dicretising a system. Knowing this, it makes sense that for the steady-state part the predictions are accurate as the same value is reached in steady state and that a smaller timestep yields better results. For the final steady state value, nothing has changed and the output is identical.

Method k =	0	1	2	3	4	5
Euler	0	0.0151	0.0281	0.0398	0.0503	0.0599
Exact	0	0.0144	0.0274	0.0392	0.0498	0.0594

Table 6-1: Steps 0 to five when comparing the Euler approximation method to the exact method of discretisation

Method k =	6	7	8	9	10
Euler	0.0685	0.0764	0.0834	0.0898	0.0956
Exact	0.0681	0.0760	0.0831	0.0895	0.0953

Table 6-2: Steps six to ten when comparing the Euler approximation method to the exact method of discretisation

Comparing the first 10 steps of the two methods yields the following results, shown in tables 6-1 and 6-2, when calculating the next step of the longitudinal velocity $\dot{x}$

Delving deeper into both MATLAB and discretisation, the c2d command of MATLAB uses the exact method to calculate the discretised system from the continuous system and thus the discretisation is implemented using the c2d command in MATLAB.

Using the c2d command, the discretised system is calculated from the continuous system. To calculate the discretised system the real values, of which d_{long} and d_{lat} are tuned in chapter 5, are used in the continuous system. The filled-in continuous system matrices are shown in the following equations:

$$A = \begin{pmatrix} -7.263 & 0 & 0 \\ 0 & -26.638 & 0 \\ 0 & 0 & -23.31 \end{pmatrix} \tag{6-7}$$

$$B = \begin{pmatrix} 0.3559 & 0.3559 \\ 0 & 0 \\ 2.227 & -2.227 \end{pmatrix} \tag{6-8}$$

$$\tag{6-9}$$

And the discretised matrices look like this, with dT being $\frac{1}{F_{imu}} = \frac{1}{72}$ as this is the sampling frequency of the IMU:

$$A_d = \begin{pmatrix} 0.9053 & 0 & 0 \\ 0 & 0.6942 & 0 \\ 0 & 0 & 0.7275 \end{pmatrix} \tag{6-10}$$

$$B_d = \begin{pmatrix} 0.0046 & 0.0046 \\ 0 & 0 \\ 0.02615 & -0.02615 \end{pmatrix} \tag{6-11}$$

$$\tag{6-12}$$

This leads to the following discretised state space equation, which is used in the next chapter to predict the next step of the velocity state and to compute the noise:

$$
\begin{pmatrix} \dot{x} \\ \dot{y} \\ \dot{\varphi} \end{pmatrix} [k+1]) = \begin{pmatrix} 0.9053 & 0 & 0 \\ 0 & 0.6942 & 0 \\ 0 & 0 & 0.7275 \end{pmatrix} \begin{pmatrix} \dot{x} \\ \dot{y} \\ \dot{\varphi} \end{pmatrix} [k] + \begin{pmatrix} 0.0046 & 0.0046 \\ 0 & 0 \\ 0.02615 & -0.02615 \end{pmatrix} \begin{pmatrix} \omega_r \\ \omega_l \end{pmatrix} [k] + w[k]
$$

$$(6\text{-}13)$$

To check the discretised system still has a satisfactory performance, the output of the longitudinal, lateral and rotational velocity for the simulation with input velocity v1 is shown in comparison to the measured experimental values for experiment 1 at input velocity v1 in Figures 6-1, 6-2 and 6-3. Comparing these to Figures 5-13, 5-15 and 5-5 show that the dicretised linear model performs as well as the continuous model. Which means that it models the rotational velocity fairly accurate, which is to be expected since the continuous model is optimised to approach the experimental values for the rotational velocity as accurately as possible. The longitudinal velocity is far of, which is also the case in the continuous model, and the lateral velocity is still zero, which is also the case in the continuous model.
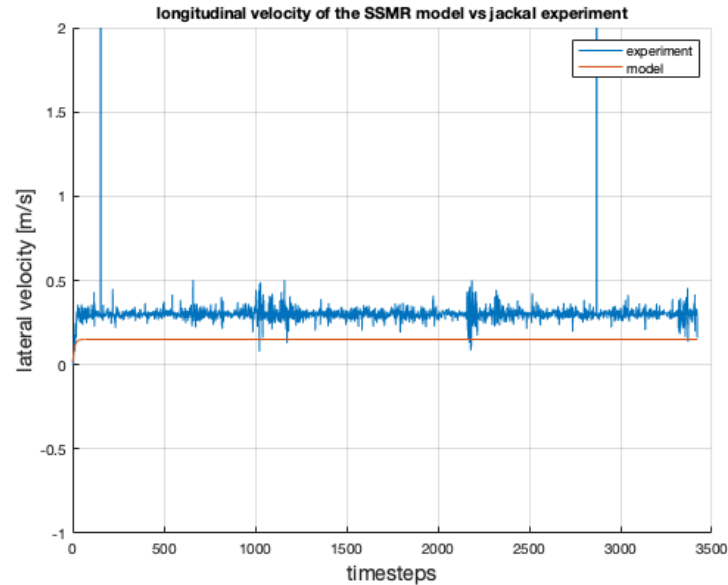
Figure 6-1: Longitudinal velocity $\dot{x}$ of the discretised model and the experimental values for the longitudinal velocity

The same check can be done for experiment 11 which uses input velocity v2. Figures 6-1, 6-2 and 6-3 can be compared to Figures 5-13, 5-15 and 5-5, which again show that the dicretised linear model performs as well as the continuous model.
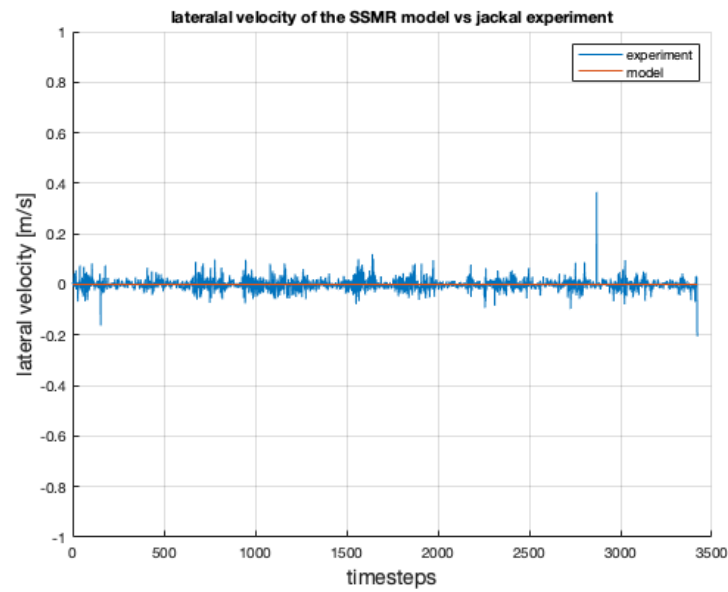
Figure 6-2: Lateral velocity $\dot{y}$ of the discretised model and the experimental values for the lateral velocity
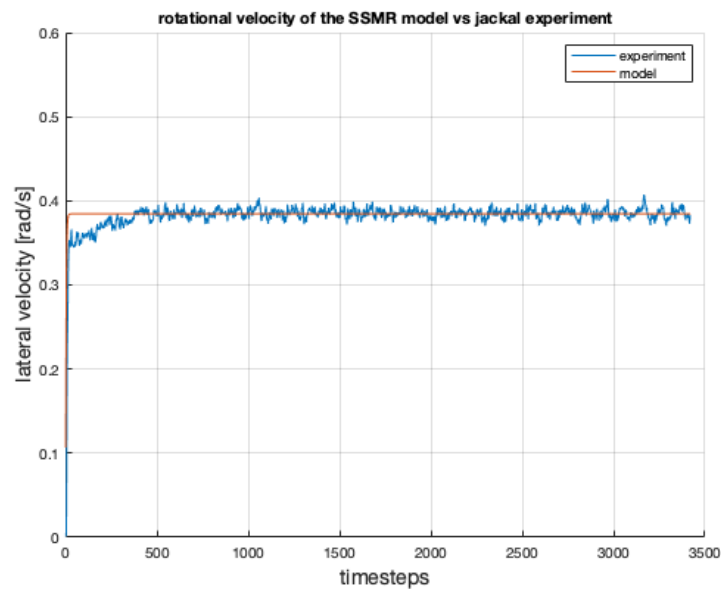
Figure 6-3: Rotational velocity $\dot{\varphi}$ of the discretised model and the experimental values for the rotational velocity
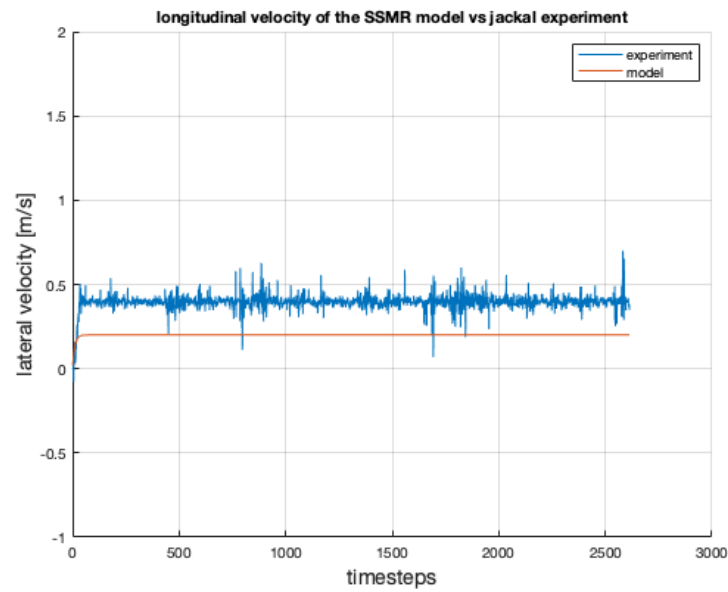
Figure 6-4: Longitudinal velocity $\dot{x}$ of the discretised model and the experimental values for the longitudinal velocity
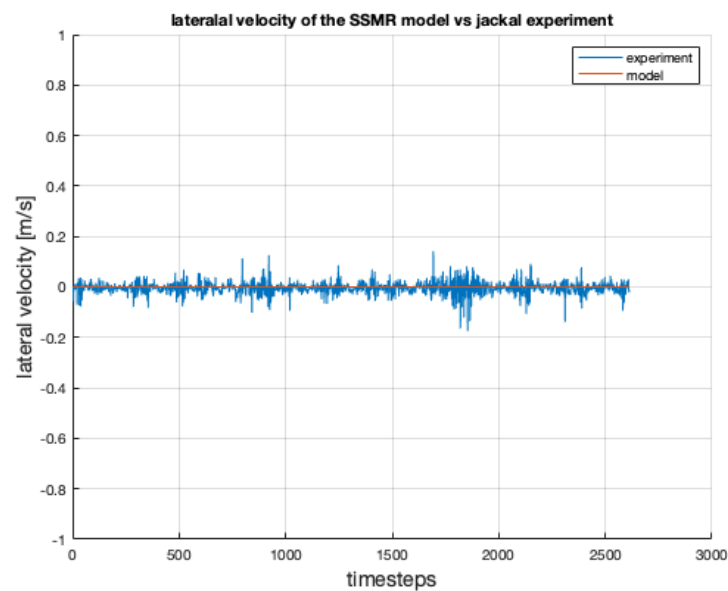
Figure 6-5: Lateral velocity $\dot{y}$ of the discretised model and the experimental values for the lateral velocity
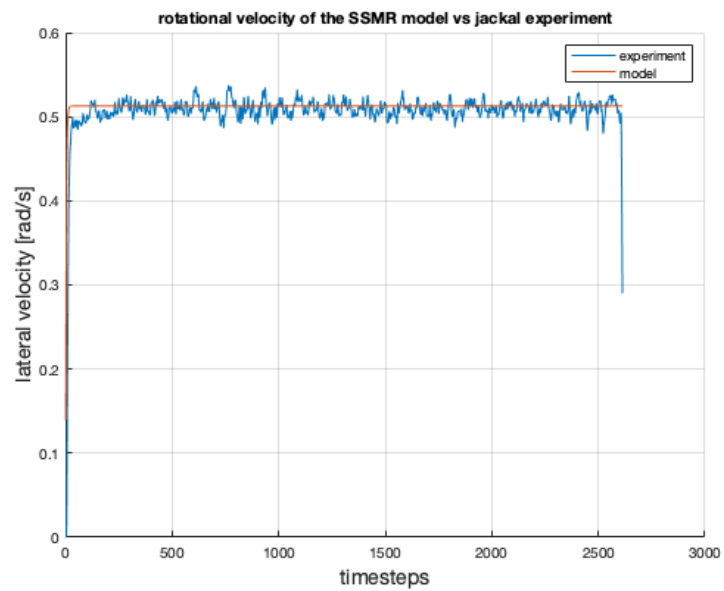
Figure 6-6: Rotational velocity $\dot{\varphi}$ of the discretised model and the experimental values for the rotational velocity

Chapter 7

Noise and Filters

This chapter answers the following sub-questions:

- *Is coloured noise present in the dynamical behaviour of the jackal robot?*

- *Can a Gaussian filter be made which recreates the coloured noise present and what are its characteristics?*

To answer these two questions, the discretised linear dynamical model is used in conjunction with the experimental data to get the estimated next step state $[k+1]_{est}$ and the difference between the estimated next step and the experimental value for $[k+1]_{exp}$ is used to compute the noise on the next step state prediction. This noise is then analyzed in this chapter and a Gaussian filter will be fitted onto the noise in order to derive a filter which will lead to the creation of coloured noise which is present in the jackal.

7-1 Noise model definition

The noise from the continuous MATLAB model is defined in the following equation, in which w is the noise due to the unmodeled dynamics in the discretised system:

$$\mathbf{x}[k+1] = A_d \mathbf{x}[k] + B_d u[k] + w[k] \tag{7-1}$$

Which is the following equation for the discretised linear dynamical system of the jackal when all values of the disctretised matrices are substituted in the system:

$$\begin{pmatrix} \dot{x} \\ \dot{y} \\ \dot{\varphi} \end{pmatrix} [k+1]) = \begin{pmatrix} 0.9053 & 0 & 0 \\ 0 & 0.6942 & 0 \\ 0 & 0 & 0.7275 \end{pmatrix} \begin{pmatrix} \dot{x} \\ \dot{y} \\ \dot{\varphi} \end{pmatrix} [k] + \begin{pmatrix} 0.0046 & 0.0046 \\ 0 & 0 \\ 0.02615 & -0.02615 \end{pmatrix} \begin{pmatrix} \omega_r \\ \omega_l \end{pmatrix} [k] + w[k] \tag{7-2}$$

The next step is to express the noise w in terms of the linear dynamical state-space model, which is done in the next equation:

$$w[k] = \mathbf{x}[k+1] - A_d\mathbf{x}[k] - B_d u[k] \tag{7-3}$$

Again, for the discretised linear dynamical system of the jackal, this leads to the following equations:

$$w = \begin{pmatrix} \dot{x} \\ \dot{y} \\ \dot{\varphi} \end{pmatrix}[k+1]) - \begin{pmatrix} 0.9053 & 0 & 0 \\ 0 & 0.6942 & 0 \\ 0 & 0 & 0.7275 \end{pmatrix}\begin{pmatrix} \dot{x} \\ \dot{y} \\ \dot{\varphi} \end{pmatrix}[k] - \begin{pmatrix} 0.0046 & 0.0046 \\ 0 & 0 \\ 0.02615 & -0.02615 \end{pmatrix}\begin{pmatrix} \omega_r \\ \omega_l \end{pmatrix}[k] \tag{7-4}$$

This is the expression for the noise in this model. By using the measured data at step $[k]$ and $[k+1]$ and the discretised matrices of the model, the process noise w can be calculated for each of the performed experiments.

The next Figures 7-1, 7-2 and 7-3 show the noise of the longitudinal, lateral and rotational velocity in the body frame of the jackal robot for experiment 1 at input velocity v1. This is the process noise present due to unmodeled dynamics.
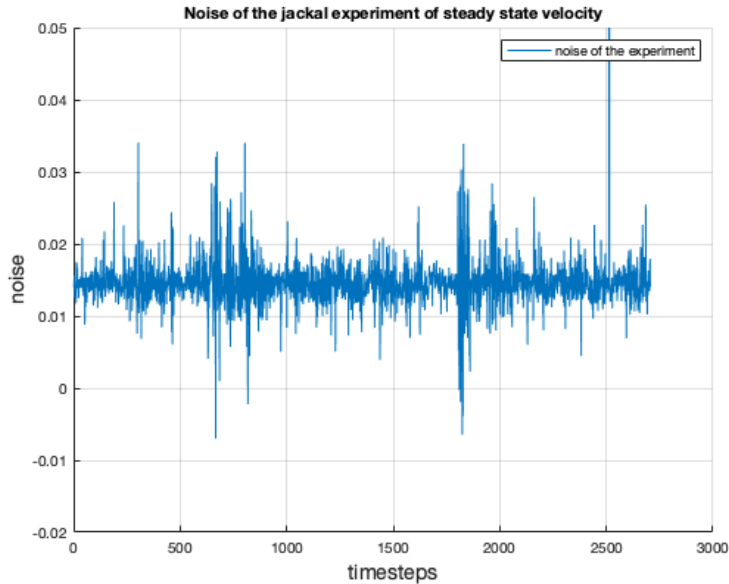
Figure 7-1: Noise of longitudinal velocity in experiment 1

Figures 7-4, 7-5 and 7-6 show the noise of the longitudinal, lateral and rotational velocity in the body frame of the jackal robot for experiment 11 at input velocity v2. This is the process
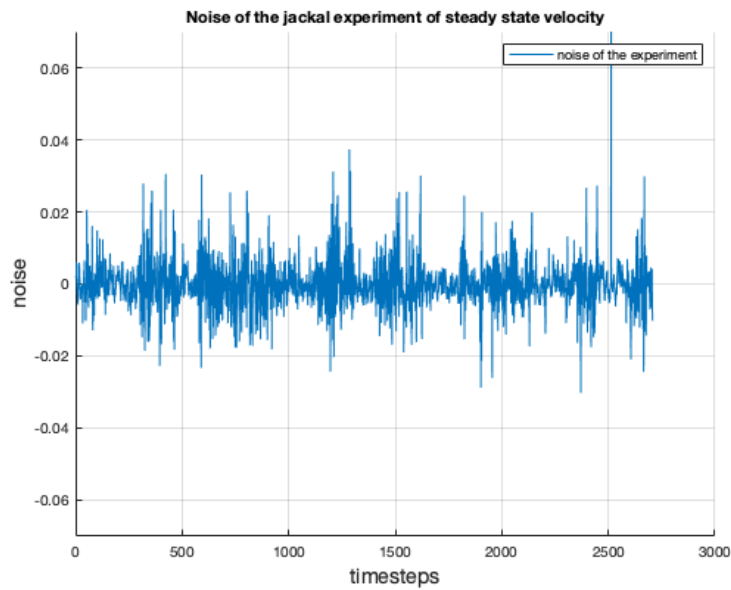
Figure 7-2: Noise of lateral velocity in experiment 1
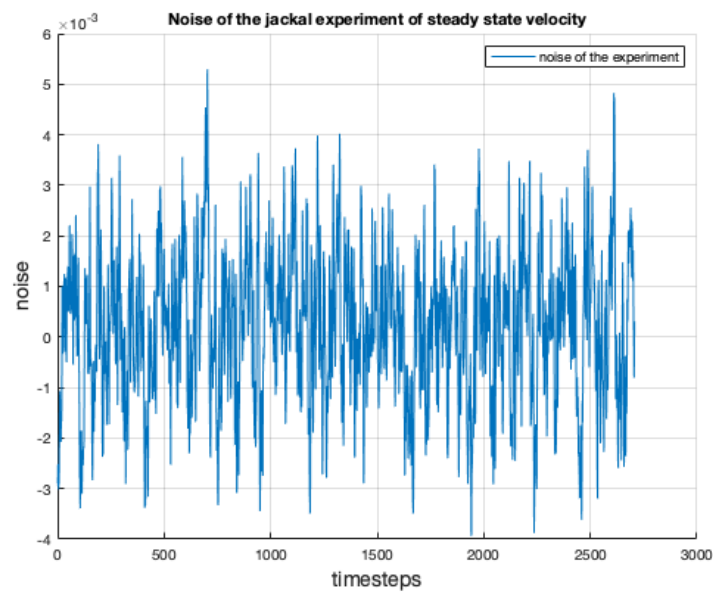
Figure 7-3: Noise of yaw rate in experiment 1

noise present due to unmodeled dynamics.

The most accurate measure for the velocity noise is presumed to be the noise of $\dot{\varphi}$, as this is the only part of the total velocity state that can be read directly from the IMU sensor of the Jackal in the experimental setup. Both $\dot{x}$ and $\dot{y}$ have to be differentiated from the position data of the motion capturing system and then resampled to match the sampling frequency
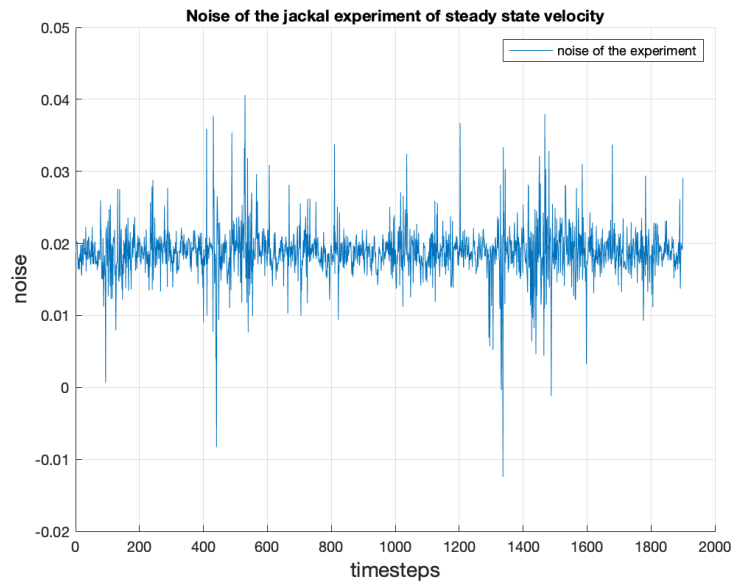
Figure 7-4: Noise of longitudinal velocity in experiment 11
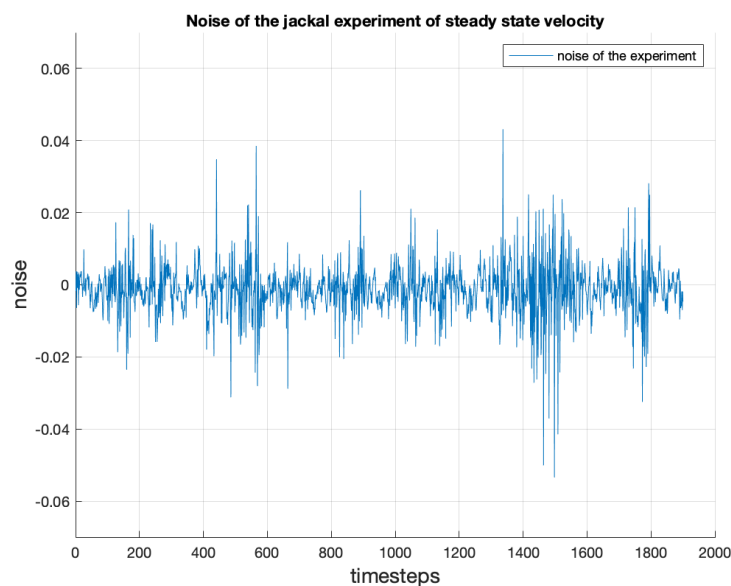
Figure 7-5: Noise of lateral velocity in experiment 11

of the IMU to get the experimental value for that state at step $[k]$. From Figures 7-1, 7-2 it is not very clear that noise is coloured. When comparing those figures to Figure 7-3, the noise signal for $\dot{\varphi}$ seems to be filtered and/or having a structure whilst the noise for both $\dot{x}$ and $\dot{y}$ looks much more uniformly distributed. Most probably this is due to the manipulation of the position data to obtain the velocity data which is usable. This is apparent in all the experiments, regardless of input velocity.
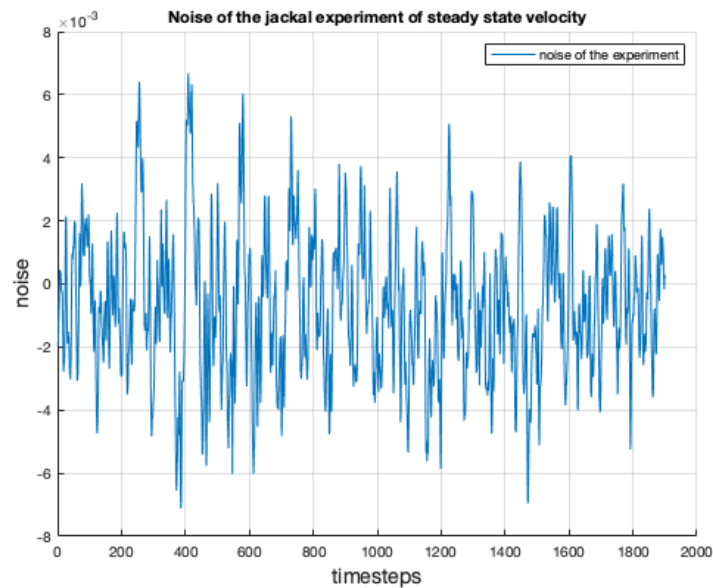
Figure 7-6: Noise of yaw rate in experiment 11

Another remark is that the steady state behaviour of the system is evaluated and graphically presented. Therefore the acceleration and deceleration part of the simulation are left out in the noise analysis.

7-2 Noise analysis

7-2-1 Rotational velocity

Figure 7-9 and 7-12, belonging to experiment 1 at input velocity v1, show that the noise is not white noise but has a structure to it and thus the noise on the rotational velocity is coloured. The magnitude plot shows that the lower frequencies are dominant and habe higher magnitudes than the higher frequencies. The autocorrelation supports this coloured noise as there is a decreasing slope as the lags grow larger. If the noise would have been white without a structure the autocorrelation for lags unequal to 0 would be very low and fall in between the confidence bounds visible in the figures. The Figures 7-15 and 7-18, which belong to experiment 11 at input velocity v2, show the same behaviour, lower frequencies are dominant in the magnitude plot and autocorrelation is present, indicating coloured noise.

7-2-2 Longitudinal and lateral velocity

From the magnitude spectrum show in Figure 7-7 and 7-8, belonging to experiment 1 at input velocity v1, it is clear that the magnitude for all frequencies is roughly equal. The autocorrelation in Figures 7-10 and 7-11 show a peak at zero and very small to non-existent peaks for bigger lags. Both are clear indications that the noise is not coloured but white noise.

Figures 7-13, 7-14, 7-10 and 7-11, belonging to experiment 11 at input velocity v2, exhibit the same behaviour: equal magnitude across all frequencies and again almnost no autocorrelation is present for lags bigger than 0.
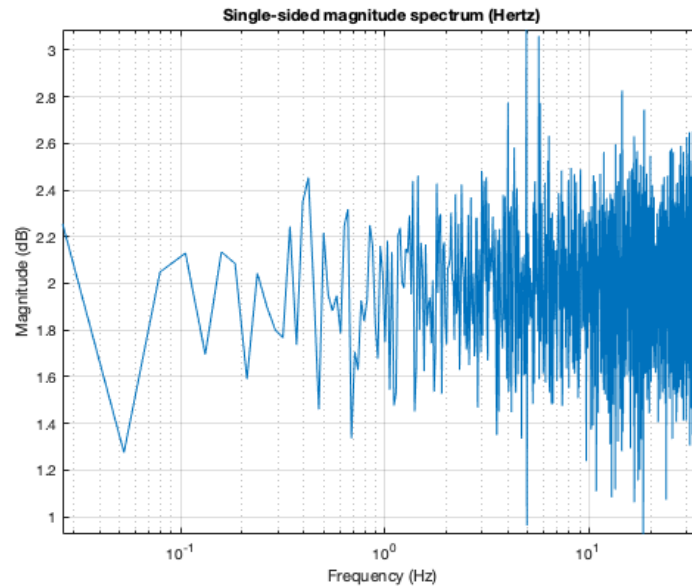
Figure 7-7: Magnitude of noise of longitudinal velocity in experiment 1
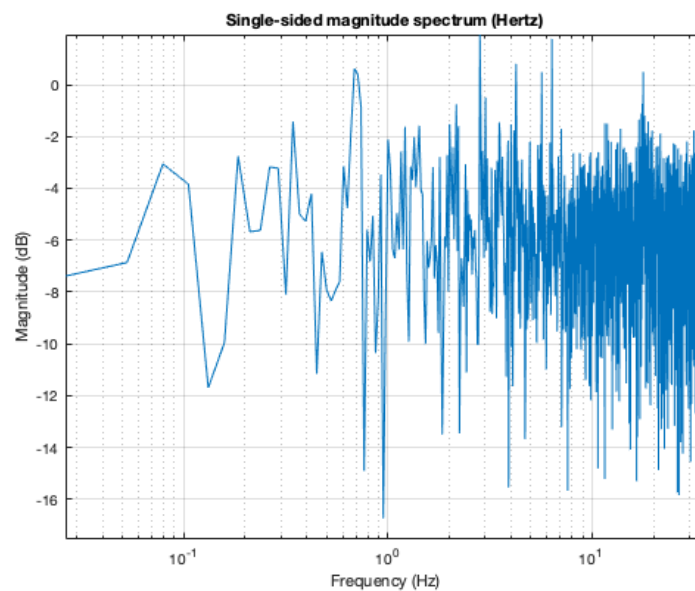
Figure 7-8: Magnitude of noise of lateral velocity in experiment 1

This leads to the conclusions that coloured noise is present in the rotational velocity of the jackal, but the presence of coloured noise for the longitudinal and rotational velocity has not been proven. This is most likely due to differentiating and re-sampling of the motion
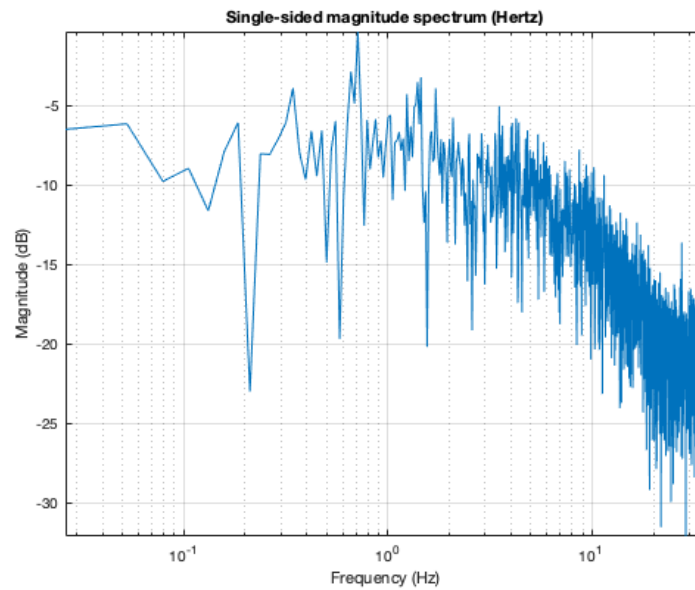
Figure 7-9: Magnitude of noise of yaw rate in experiment 1
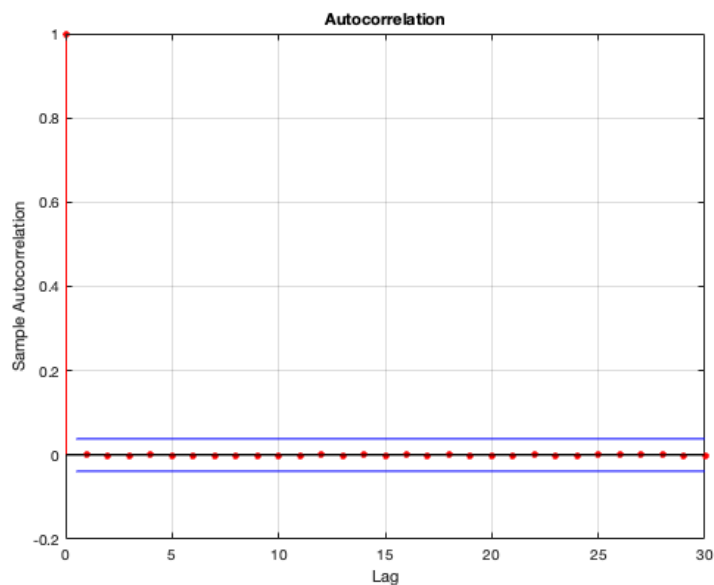
Figure 7-10: Autocorrelation of the noise of longitudinal velocity in experiment 1

capturing data. Differentiating and resampling results in a noisy signal which could possibly mask any colour present in the noise. It is recommended to try and obtain the longitudinal and lateral velocities in a different manner, possible combining the information from the IMU and the motion capturing system for a more accurate representation of the velocities.

Now that there is proof that coloured process noise occurs during steady state cornering of
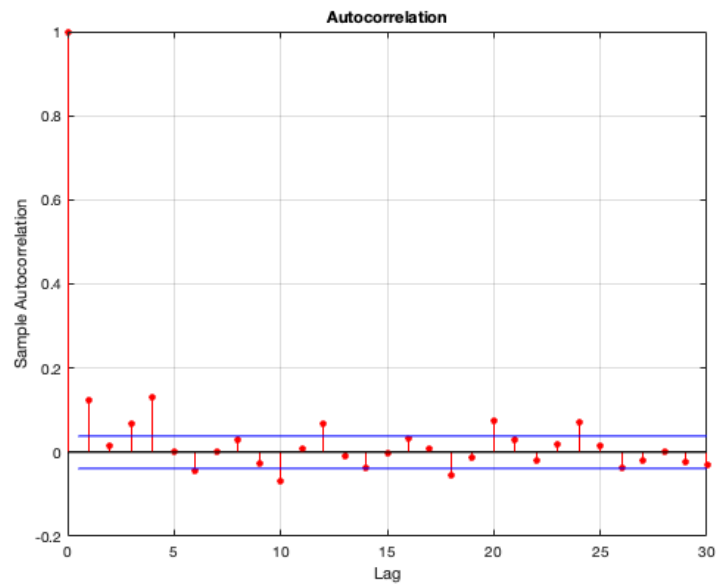
Figure 7-11: Autocorrelation of the noise of lateral velocity in experiment 1
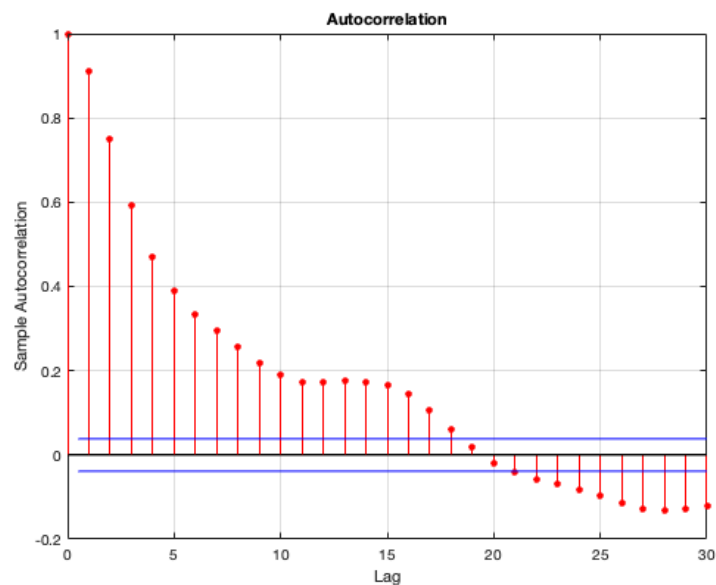
Figure 7-12: Autocorrelation of the noise of yaw rate in experiment 1

the jackal robot exists for the rotational velocity, a filter can be made which can emulate the characteristics of the coloured process noise on the rotational velocity. This is filter H_w which can be seen in Figure 7-19. Note, the process noise z is assumed to significantly bigger than the measurement noise, therefore the measurement noise will be ignored and no filter H_z will be fitted
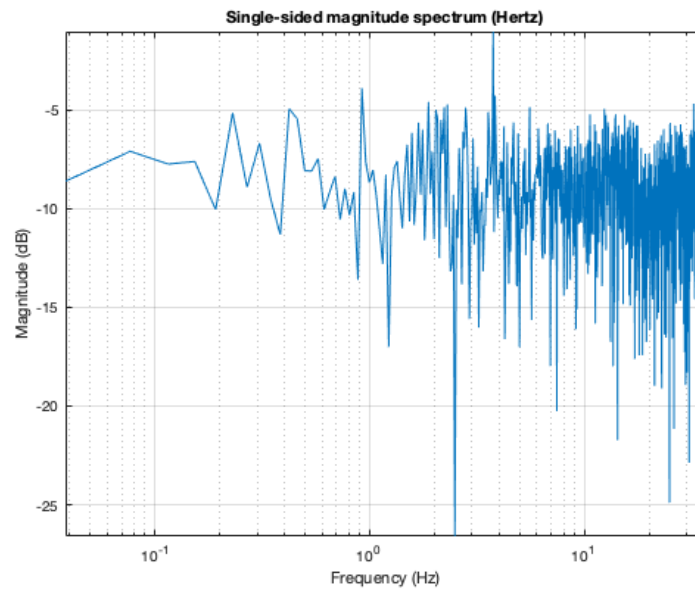
Figure 7-13: Magnitude of noise of longitudinal velocity in experiment 11
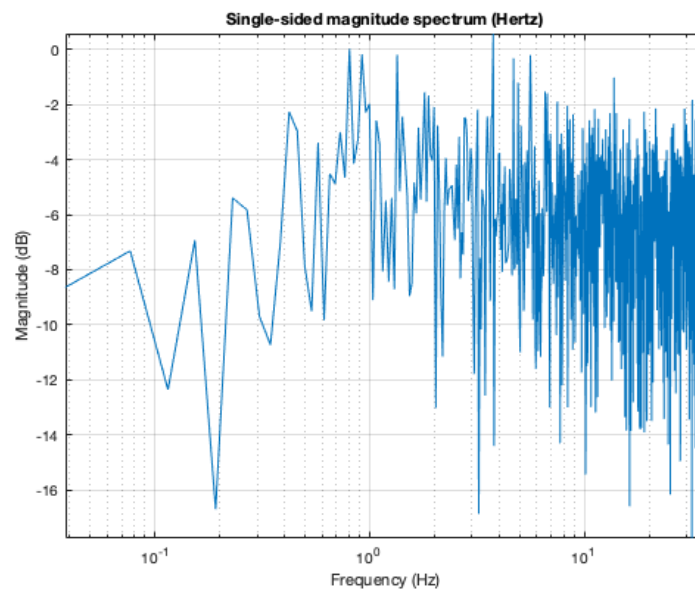
Figure 7-14: Magnitude of noise of lateral velocity in experiment 11

7-3 Filters and fitting

The final piece of this research is to answer the question if it is possible to get an estimate for a filter which filters white noise in such a way that the output of the filter resembles the coloured noise on the rotational velocity measured in the jackal. In Active Inference, a Gaussian filter is used to create the needed coloured noise from white noise. As the goal for this research is to identify and analyze coloured noise to show that the jackal system is
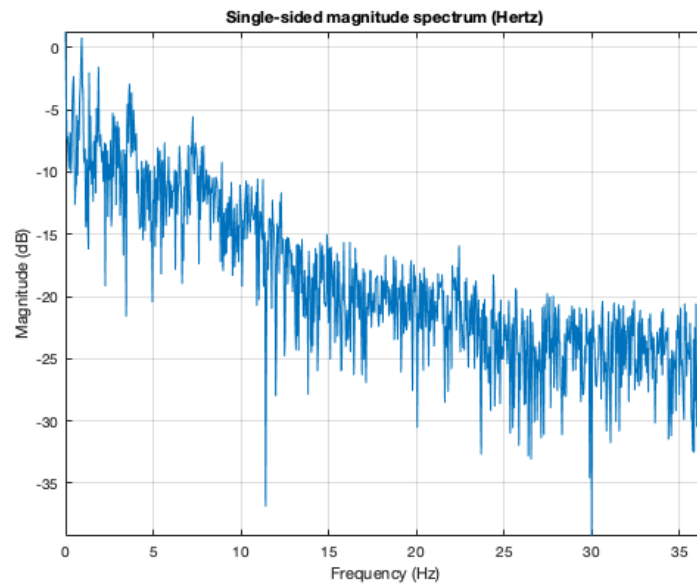
Figure 7-15: Magnitude of noise of yaw rate in experiment 11
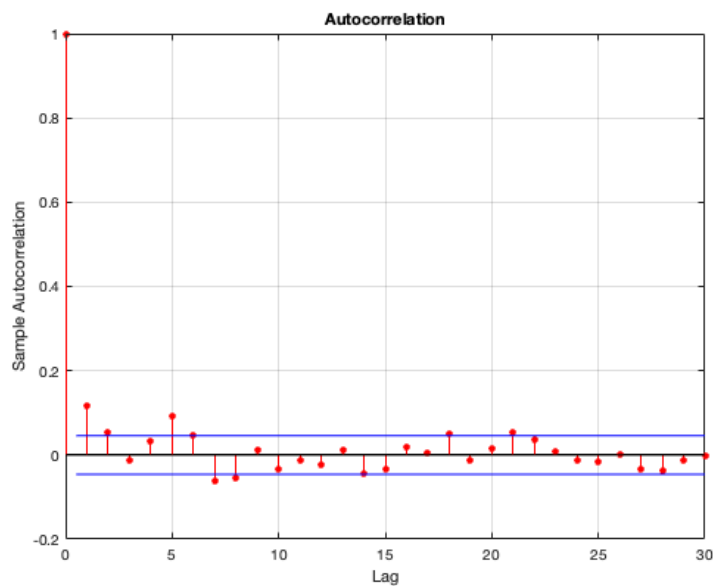
Figure 7-16: Autocorrelation of the noise of longitudinal velocity in experiment 11

a useful case to demonstrate Active Inference on, the Gaussian filter will be fitted on the coloured noise of the rotational velocity of the jackal.

7-3-1   Gaussian-filter

The Gaussian filter used to recreate coloured noise is described by M. Wisse [16]. Equation 7-5 shows the Gaussian filter
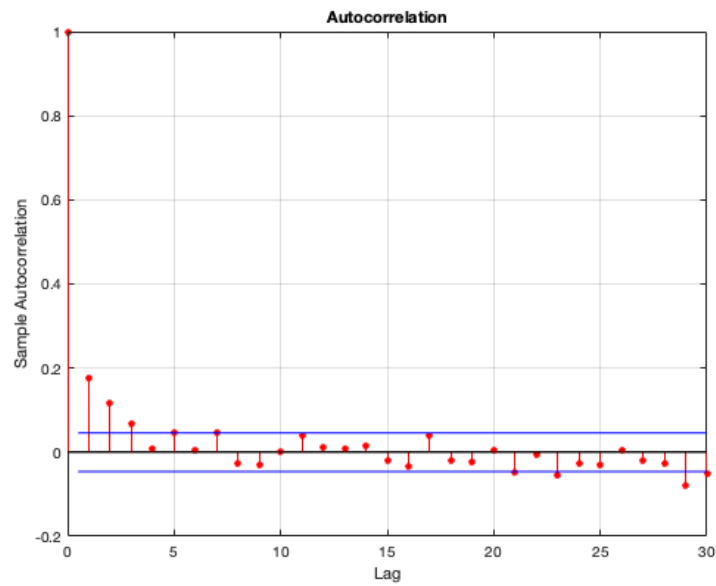
Figure 7-17: Autocorrelation of the noise of lateral velocity in experiment 11
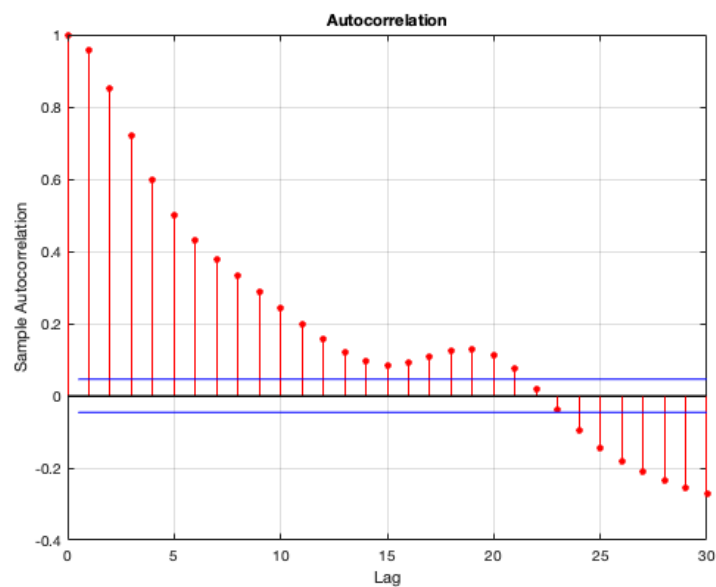
Figure 7-18: Autocorrelation of the noise of yaw rate in experiment 11

$$h(t) = \sqrt{\frac{dT}{\sigma_h \sqrt{\pi}}} e^{-\frac{\tau^2}{2\sigma_h^2}} \qquad (7\text{-}5)$$

The equations contains parameters of which some can be tuned to recreate the coloured noise present in the jackal. The most important parameter to be tuned is the kernel width σ_h.
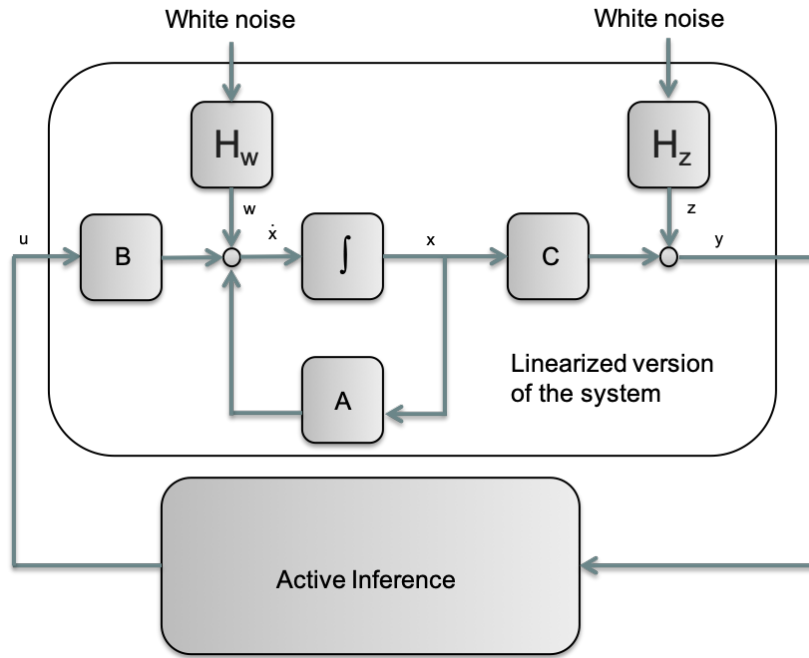
Figure 7-19: Block scheme of the physical system and Active Inference, the filter H_σ which is to be determined can be seen in the upper left corner of the system block diagram.

The kernel width determines the shape of the Gaussian and the size of the filter as it is good practice to set the size of the filter as wide as six times the kernel width [17], in this case σ_h. This is done to ensure that the values in the Gaussian kernel account for three standard deviations to the left of the center and three standard deviations to the right of the center of the Gaussian to account for 99.73% of the set of values within the Gaussian. This is graphically represented in Figure 7-20.
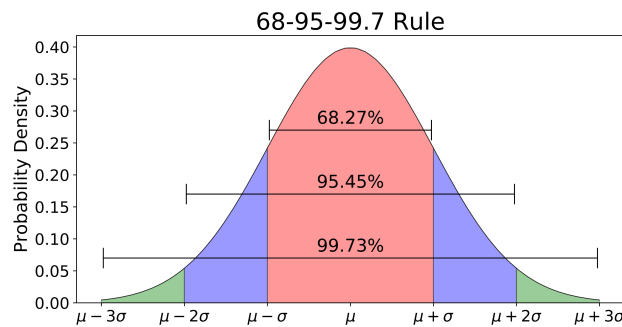
Figure 7-20: Gaussian distribution [18] which shows that a total size of 6 σ_h is needed to account for 99.73% of the Gaussian in filtering

The parameter dT in the equation of the Gaussian corresponds to the sample time of the signal. The rotational velocity was recorded using the internal IMU of the jackal which has a sampling frequency of $72Hz$ and thus a sampling time dT of $\frac{1}{72}$ s.

Utilizing the following property of filters, when filtering white noise with a Gaussian filter,

the resultant filtered noise has the same autocorrelation as the autocorrelation of the impulse response of the Gaussian filter, the Gaussian can be fitted onto the coloured noise found in the jackal. This is done in four steps: The first step is to denote the noise signals in time instead of number of samples. The next step is to compute the autocorrelation of the coloured noise measured for all fifteen experiments for the first 30 lags of the signal. The second step is to create a white noise signal and to filter that white noise signal with a Gaussian filter with a certain σ_h to compute the autocorrelation of the output of the filtered white noise for the first 30 lags. Note, it would be more precise to directly used the impulse response of the Gaussian filter, less artefacts are introduced and for a perfect representation of white noise the signal would have to be infinitely long. Such a signal cannot be made. To get an approximation of the infinitely long signal, a very large time signal is created, order of magnitude of a 1000 times longer than the length of the time signals of the measured noise. This should suffice as an approximation. This approach was chosen because of computational efficiency. The third and final step is to compute the mean squared error (MSE) of those two autocorrelations, which can be seen in the following equation with l being the number of lags considered in the autocorrelation, with $MAGJ$ representing the magnitude of the autocorrelation at each lag l for the jackal and $MAGF$ representing the magnitude for the autocorrelation at each lag l for the Gaussian filter:

$$MSE = \frac{1}{l}\Sigma_{i=1}^{l}\Big(MAGJ_l - MAGF_l\Big)^2 \tag{7-6}$$

This is done for a range of σ_h, spanning from **0.001 to 1, in increments of 0.001**. This range is chosen by looking at the report in which this specific Gaussian filter is described [16]. In this report, σ_h has a value of 0.1 as an example, but more importantly, it states that σ_h is chosen to be larger than the sampling time but smaller than simulation time. The range of 0.001 to 1 in increments of 0.001 does not fully adhere to these statements, the lower bound is smaller than the sampling time of $0.014s$ but the upper bound is indeed smaller than the duration of around 38 seconds for the experiments with input velocity v1 or around 26 seconds for the experiments which use input velocity v2 as an input.

From Figure 7-21 the optimal values for σ_h can be seen for the experiments with input velocity v1, the experiments with input velocity v2 and for all experiments combined. The values have been averaged for each input velocity over all experiments which use that input velocity, except of-course when all experiments all combined, regardless of input velocity. Table 7-1 depicts the exact values for σ_h and τ. Each value for σ_h is accompanied by a value for τ as that is chosen as dependent on σ_h.

velocity	state	σ_h
v1 rotational	$\dot{\varphi}$	0.051
v2 rotational	$\dot{\varphi}$	0.041
all exp rotational	$\dot{\varphi}$	0.047

Table 7-1: The values for σ_h averaged over the experiments with input velocity v1 and v2

The values found for σ_h in Table 7-1, when averaged over all experiments, translate into the following Gaussian filter when the values for σ_h and dT are substituted in equation 7-5:
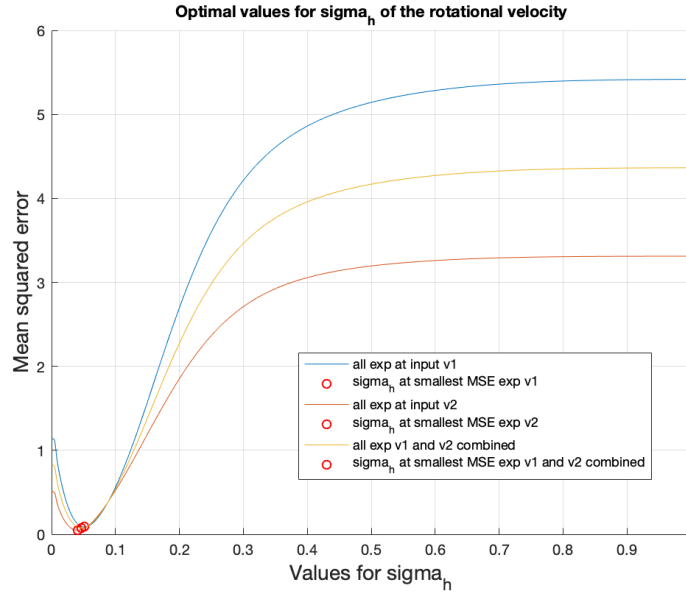
Figure 7-21: For the rotational velocity $\dot{\varphi}$ and each input velocity v1 and v2 used in the experiments a range of σ_h is fitted to find the value for σ_h which yields the lowest MSE between the autocorrelations of the coloured noise of the jackal and the autocorrelation of the noise after white noise has been filter with the Gaussian filter

$$h_{\dot{\varphi}}(t) = \sqrt{\frac{0.014}{0.047\sqrt{\pi}}} e^{-\frac{\tau^2}{0.094^2}} \tag{7-7}$$

7-4   Noise comparison

When looking at the autocorrelation plots of the noise signals, the comparison between the created noise and the found noise for the rotational velocity can be seen in Figures 7-22, 7-23 and 7-24.

The created noise fails to exactly recreate the autocorrelation of the coloured noise in the jackal for all 30 lags but it yields an acceptable estimate given the fact that it is fitted to 15 experiment using two different velocities. For the first six lags the magnitudes correspond roughly but the shape of the autocorrelation differs slightly after lag 6. This might indicate that the Gaussian filters, after optimizing σ_h are not able to fully capture the characteristics of the coloured and further investigation into different kinds of filtered is recommended. The rest of the autocorrelation figures of all experiments can be seen in Appendix A.
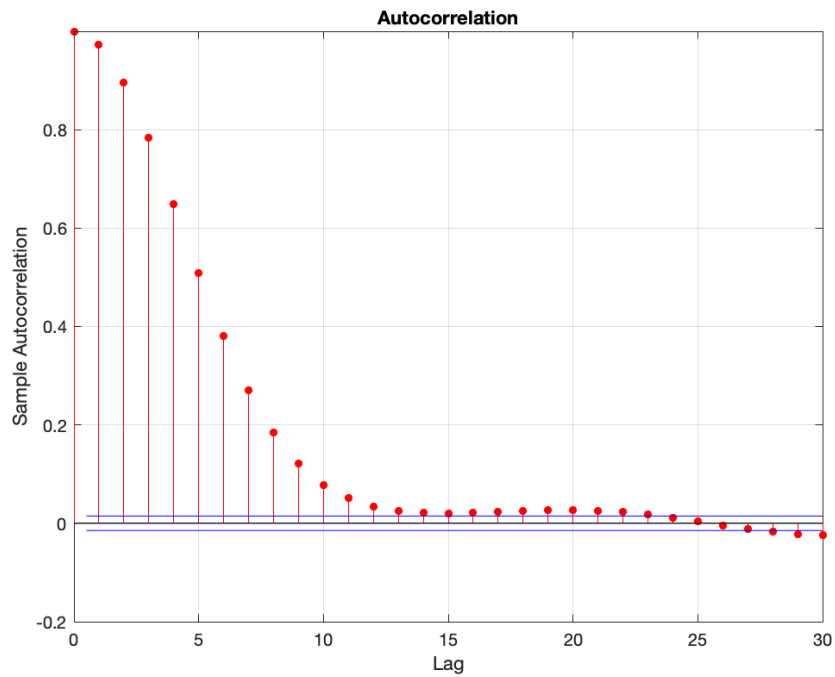
Figure 7-22: Magnitude plot of filtered white noise for the rotational velocity
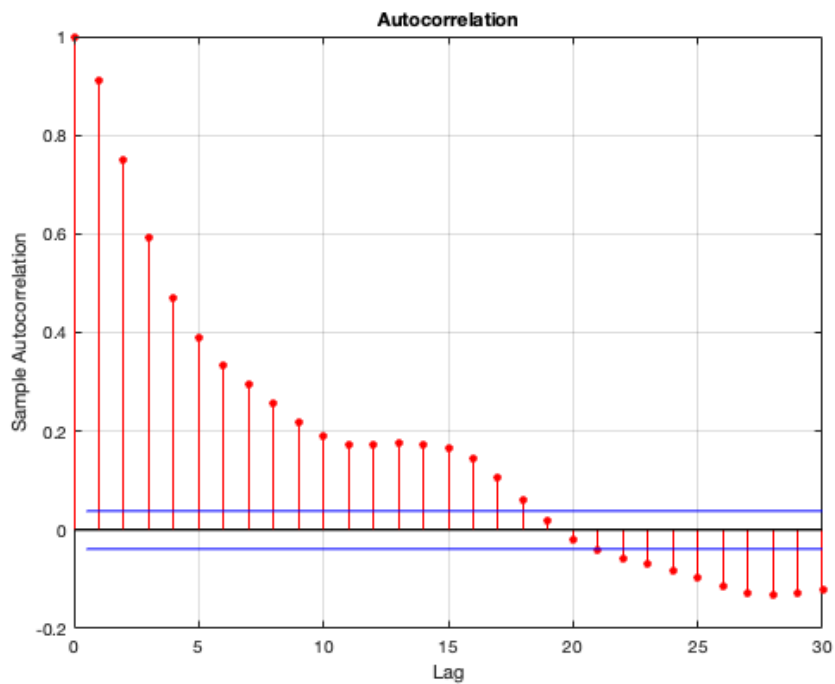
Figure 7-23: Autocorrelation of measured coloured noise in the jackal for the rotational velocity in experiment 1 at input velocity v1
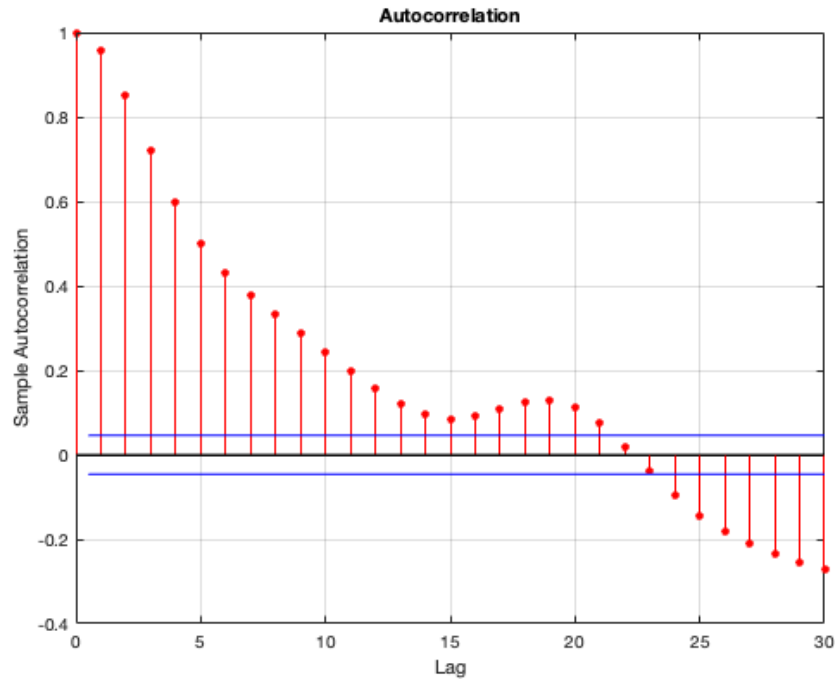
Figure 7-24: Autocorrelation of measured coloured noise in the jackal for the rotational velocity in experiment 11 at input velocity v2

7-4-1 Further filter recommendations

The Gaussian filter is not the only filter which could be able to recreate the coloured noise found during the experiments with the jackal. The magnitude plots of the noise on rotational velocity shows a higher magnitude for lower frequencies in all experiments at both input velocities. Taking this into account, other linear filters which are low-pass filters[19] might also be able to recreate the coloured noise. Looking at the shape of the Gaussian filter a triangular filter might also be an option, the same goes for a moving average filter[19].

Non-linear filters might also be considered to recreate the coloured noise more accurately. Further research to see if other types of filters are able to more accurately recreate the coloured noise is recommended, but within the scope of this research and keeping the Active Inference framework in mind, the choice for the Gaussian filter is a logical choice.

Chapter 8

Conclusion

The main goal of the research is:

Measurement and analysis of the coloured noise on the longitudinal, lateral and rotational velocities and identifcation of its characteristics due to the unmodeled dynamics of a skid steer mobile robot during a steady-state turning manoeuvre.

The goal is partly achieved, it is proven that coloured noise on the rotational velocity is present in steady-state cornering of the jackal and the following filter is developed which characterises the coloured noise on the rotational velocity and is able to recreate the measured coloured noise in the jackal by filtering a white noise signal:

$$h_{\dot{\varphi}}(t) = \sqrt{\frac{0.014}{0.047\sqrt{\pi}}} e^{-\frac{\tau^2}{0.094^2}} \tag{8-1}$$

The three sub-goals stated in chapter 1 are also achieved and for each sub-goal a small conclusion will be stated.

Create a linear dynamical model of the jackal robot and optimize the model in such a way that its velocity states resemble the experimental values of the velocities for the given experimental inputs.
Chapters 4 and 5 describe the creation and optimization of the linear model of the jackal robot. The linear model is optimized in such a way that the output of the rotational velocity $\dot{\varphi}$ closely matches the experimental values for the rotational velocity $\dot{\varphi}$. This is done by optimizing parameters d_{lat} and d_{long}.

Show the presence of coloured noise in the dynamical behaviour of the jackal robot.
Chapter seven proves the presence of coloured noise in the rotational velocity state of the

jackal in steady-state cornering due to unmodeled dynamics. The magnitude plot for the rotational velocity state $\dot{\varphi}$ shows that the lower frequencies have a higher magnitude than the higher frequencies in the noise indicating the prevalence of noise due to unmodeled process dynamics. And the autocorrelation graph of the noise of rotational velocity state indicates the same, coloured noise is present. However for the longitudinal and lateral velocity states $\dot{x}$, $\dot{y}$, the presence of coloured noise is not proven. Magnitude plots show a equal magnitude for all frequencies present and the autocorrelation shows a very low to non-existent autocorrelation for lags greater than 0. This indicates that the measured noise is white. This is probably due to the fact that the longitudinal and lateral velocities could not be measured directly during the experiments but had to be inferred from position measurements. This introduces extra unwanted noise and because of that, coloured noise has not been measured for the longitudinal and lateral velocities.

Create a (Gaussian) filter and determine its characteristics, which can recreate the coloured noise found in the velocity states of the jackal robot in steady state turning.
Secondly, chapter seven reports on the successful creation of a Gaussian filter which is able to recreate the coloured noise in the rotational velocity state of the jackal during steady-state cornering. The characteristics for the Gaussian filter are found by optimizing the mean squared error of the difference between the autocorrelation magnitudes of the coloured noise in the jackal and the coloured noise which is created by the Gaussian filter. And thus a Gaussian filter is created which is able to reproduce the coloured noise found in the rotational velocity state of the jackal.

$$\text{Chapter} \quad 9$$

Discussion & Recommendation

During research, obstacles and problems always arise and as such, ways to combat those problems and navigate the obstacles also arise. In hindsight, with further knowledge on the subject and a better understanding of the research, recommendations can be made to improve the research and to build upon for future work regarding this subject. This topic reflects on the research done and discusses the both the results and the methods to find improvements and advice on for future work.

9-1 Discussion

9-1-1 More realistic wheel-to-surface contact model

A more realistic wheel-to-surface contact model might yield better results. The idea that the wheel-to-surface contact can be modelled by a viscous damper is an elegant and simple idea but more intricate and realistic tyre behaviour exists and is used in both research and the industry. Examples from the field of vehicle dynamics are the Lugre friction model [14] and magic tyre model [15]. However, these model have a degree on non-linearity and thus the model will have a higher degree of complexity which has its downsides such as computational requirements and the possible need to linearise the model.

9-1-2 Other optimization methods

The linear model is optimised to fit the experimental data by reducing the mean squared error between the rotational velocity of the simulation and the experimental data. This means that the rotational velocity output of the linear model matches the rotational velocity measured in the experiments as good as possible. However, in this research the prediction of the rotational velocity for each next step of the state when inputting experimental data in the model is used as a measure for the noise and not the difference between the experimental and simulated value for $\dot\varphi$. Optimizing the model in such a way that the estimation of each next step is the

most accurate might result in a different and more optimal pair of d_{lat} and d_{long}.

To verify that the optimisation used in this thesis can be used to find the optimal pair of damping coefficients d_{lat} and d_{long}, the proposed method as stated above is implemented for a single experiment which uses input velocity v1 and a single experiment which uses input velocity v2. The method is implemented in the following way.

For each pair of damping coefficients in the range of $10 - 1000$ in increments of 10, the continuous model is being discretised using the method described in chapter 6. The discretised matrices A_d and B_d are used to calculate the estimated next step state $\dot{\varphi}$ using the following equation:

$$x[k + 1] = A_d x[k] + B_d u[k] \tag{9-1}$$

The estimation is then subtracted from the experimental value of $\dot{\varphi}$ at step $[k + 1]$ and the mean squared error is calculated between the estimated and measured values of each $[k + 1]$ using the following equation:

$$MSE = \frac{1}{n} \Sigma_{i=1}^{n} \Big(x[k + 1]_{exp} - x[k + 1]_{est} \Big)^2 \tag{9-2}$$

For all possible combinations of d_{lat} and d_{long} within the of $100 - 1000$, this leads to the following results that show different optimal values for d_{lat} and d_{long}. However Figure 9-1 shows a graph which is similar in shape to Figure 5-1 in chapter 5 for the optimal values of d_{lat} and d_{long} at input velocity v1:

- $d_{lat} = 40 \ Ns/m$

- $d_{long} = 10 \ Ns/m$

For the second experiment at input velocity v2, again different results can be found when comparing to the results in chapter 5 for both the optimal values of d_{lat} and d_{long}. And again Figure 9-2 resembles the shape of Figure 5-2 in chapter 5.

- $d_{lat} = 40 \ Ns/m$

- $d_{long} = 10 \ Ns/m$

Due to the linear nature of the model, not much difference was expected when optimizing to the next step state prediction error of $\dot{\varphi}$ instead of the error of the actual value $\dot{\varphi}$. The found values however are not the same as the previous values found for d_{lat} and d_{long}. However, the ratio of 4 between d_{lat} and d_{long} is approximately the same as the ratio between the values found in Chapter 5 which was $3\frac{2}{3}$. Taking into account that the optimisation is done in increments of ten, the combination for d_{lat} and d_{long} is the closest combination that is

MMSE experiment n1 v1 vs d$_{lat}$ and d$_{long}$

Figure 9-1

MMSE experiment n11 v2 vs d$_{lat}$ and d$_{long}$
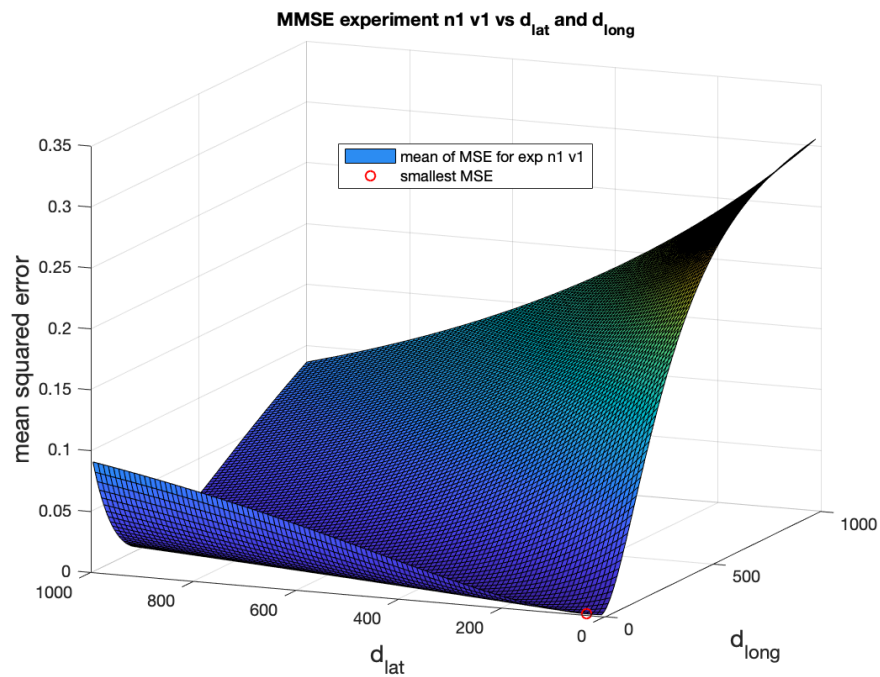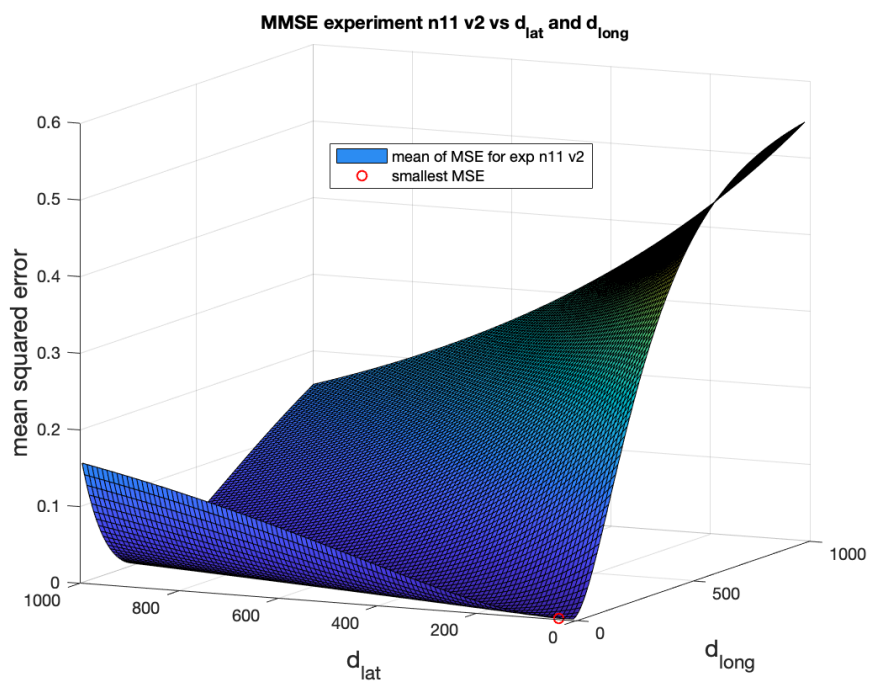
Figure 9-2

possible when taking either d_{lat} as 40 or d_{long} as 10. Furthermore, it is interesting to see that this combination also lies on the line which can be seen in Figure 5-4 in Chapter 5.

However, due to a less efficient programming loop this process was far more computationally intensive than the previous process used in chapter 5. The calculation of the optimization process for a single experiment using the next step state estimation took almost as much time as the calculation for all fifteen experiments when only calculation $\dot{\varphi}$ using a simulation of the continuous model. This might be optimised by discretising all possible continuous models outside of the loop in advance but this was out of the scope of this research.

9-1-3   Obtaining and analysing longitudinal and lateral velocity

Getting an accurate measurement for the longitudinal and lateral velocity would be a great improvement for this research. In the process of manipulating the position measurements to get the velocities a lot of unwanted and unnecessary noise was added to the inferred velocities. Another option was to use the accelerations from the IMU, but combating drift is also an obstacle when integrating accelerations to obtain velocities. For future work, it is recommended to get a more accurate reading of the longitudinal and lateral velocities. An option might be combining the acceleration measurements with the position measurements of the Optitrack system. Getting better longitudinal and lateral velocity estimates might result in proving structured noise is also present in those velocity states.

9-2   Recommendations

9-2-1   Extra experiments

To gather more real life data on the behaviour of the jackal, more and different experiments are needed. The focus for this research was on steady-state cornering behaviour of the jackal. This is done because of two reasons, in cornering slipping occurs with a skid steer mobile robot and therefor coloured noise will be present in the data. And steady-state behaviour is a very good first step into gaining an insight in the coloured noise and behaviour of the robot as it is more predictable and easier to analyse than non-steady-state behaviour. To further gain data and to test the linearised model and determine the noise characteristic of the system it is advisable to perform additional experiments with different kinds of steady-state and non steady-state manoeuvres. Examples of these experiments that could be done are:

- Performing a figure-8 motion

- Performing a rotation on the spot in both clockwise and counter clockwise rotation

- Performing manoeuvres in different locations within the motion capturing lab, different floor conditions might yield different results

- Performing the same experiments at different input velocities to determine state dependence of the data and linearised model

- Performing the same experiments with another type of skid steer mobile robot to determine the scalability of the linearise model

9-2-2 Investigate different filters

As stated in the remarks section at the end of chapter 7, future research might also expand on the notion of using a different filter to recreate the coloured noise. Other filters might yield coloured noises which are even more similar to the coloured noise occurring in the jackal but the predominance of the Gaussian filter in the field of Active Inference might be a restriction on the choice of filters.

9-2-3 Application on other skid steer mobile robots

To see if the model can be universally applied and scaled to other skid steer mobile robots further experiments must be done with other brands and types. Scaling in terms of weight, size, velocities, number of wheels might be a factor in a better or worse performance of the model when applied to other brands and types of skid steer mobile robots.

9-2-4 Applying Active Inference

The most important recommendation for future work however is the application of Active Inference on this model and on the control and state estimation of the real life jackal robot. As stated in the introduction of this report, this research on the system characteristics and model is only one part of the loop. The other part of the loop is the implementation of Active Inference on this model to really find if the combination of this simplified linear dynamical model and coloured noise characteristics suffices to control a skid steer mobile robot.

Appendix A

Additional figures from additional experiment runs

A-1 Autocorrelation of the measured noise in additional experiments at input velocity v1 and v2

In this section the autocorrelation figures of the additional nine experiments at slower input velocity v1 and v2 are shown. There are 9 additional experiments done at v1 and 4 additional experiments done at v2.
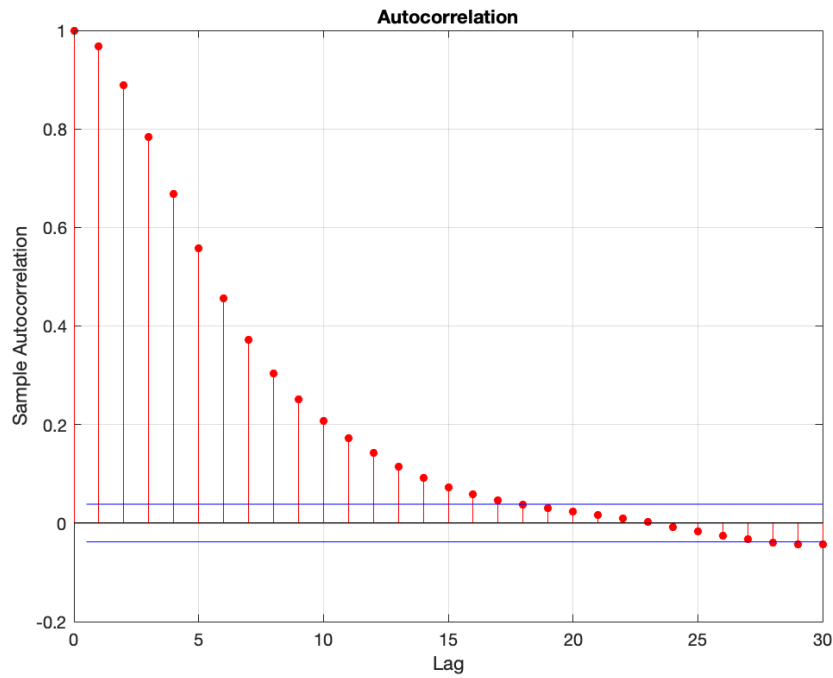
Figure A-1: Autocorrelation of measured coloured noise in the jackal for the rotational velocity in experiment 2 at input velocity v1
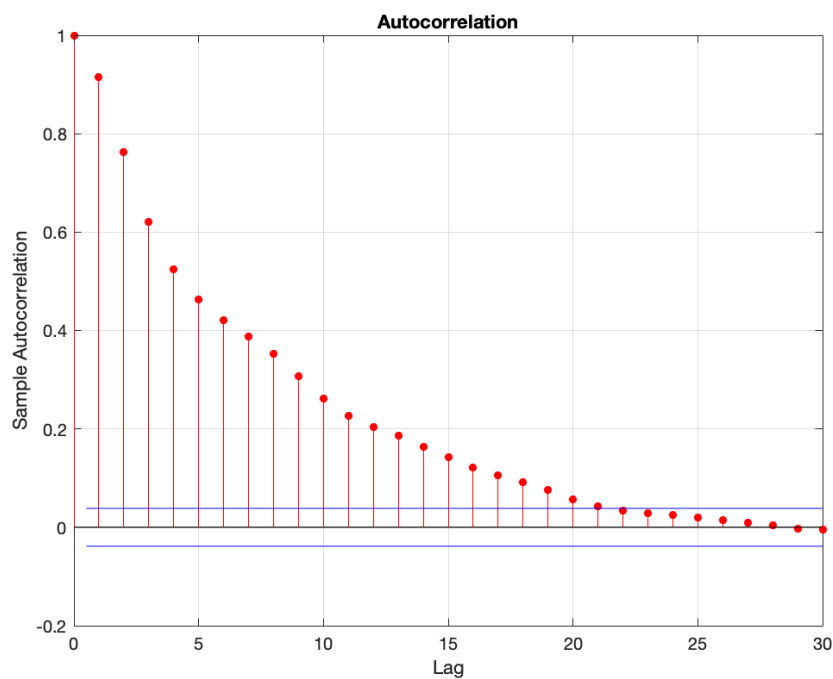
Figure A-2: Autocorrelation of measured coloured noise in the jackal for the rotational velocity in experiment 3 at input velocity v1
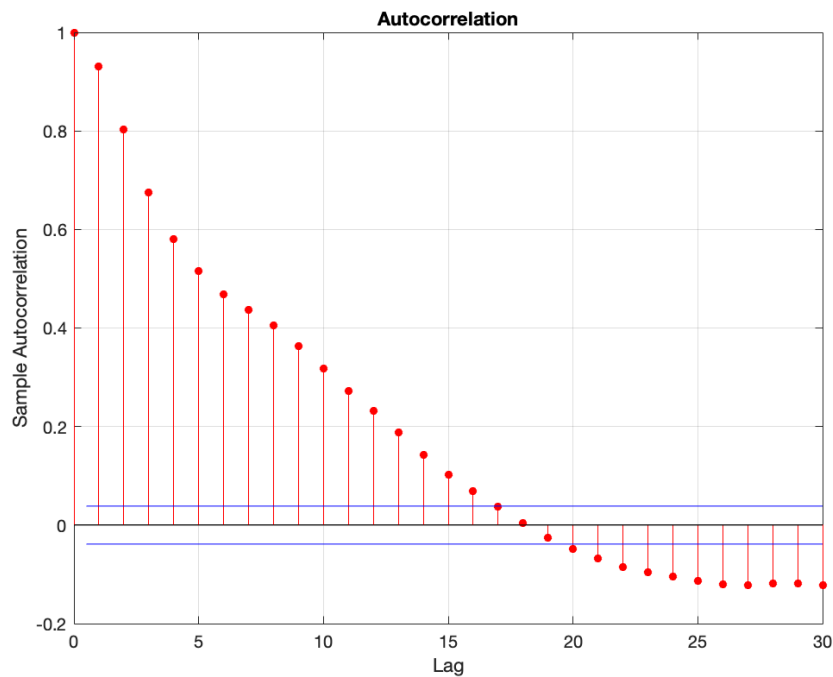
Figure A-3: Autocorrelation of measured coloured noise in the jackal for the rotational velocity in experiment 4 at input velocity v1
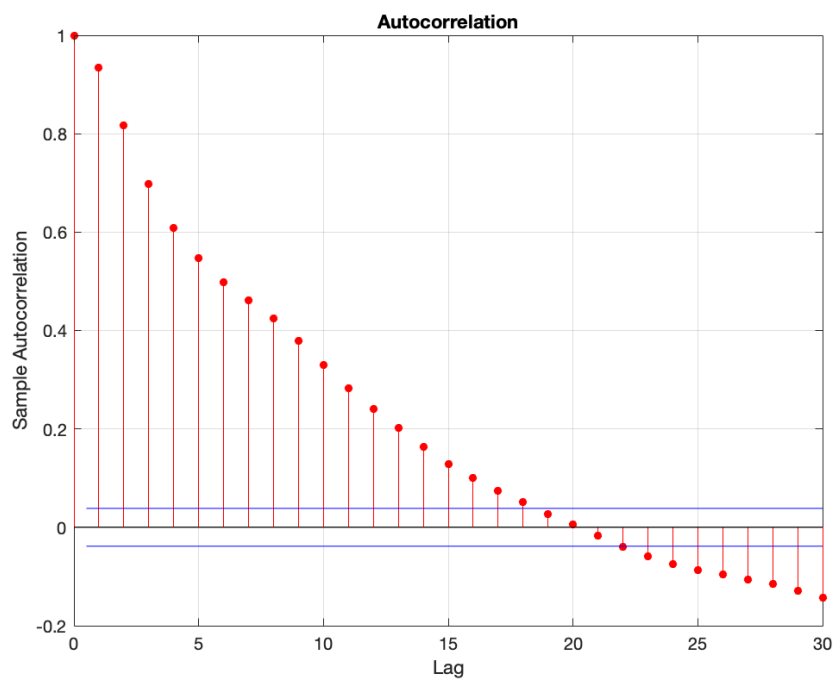
Figure A-4: Autocorrelation of measured coloured noise in the jackal for the rotational velocity in experiment 5 at input velocity v1
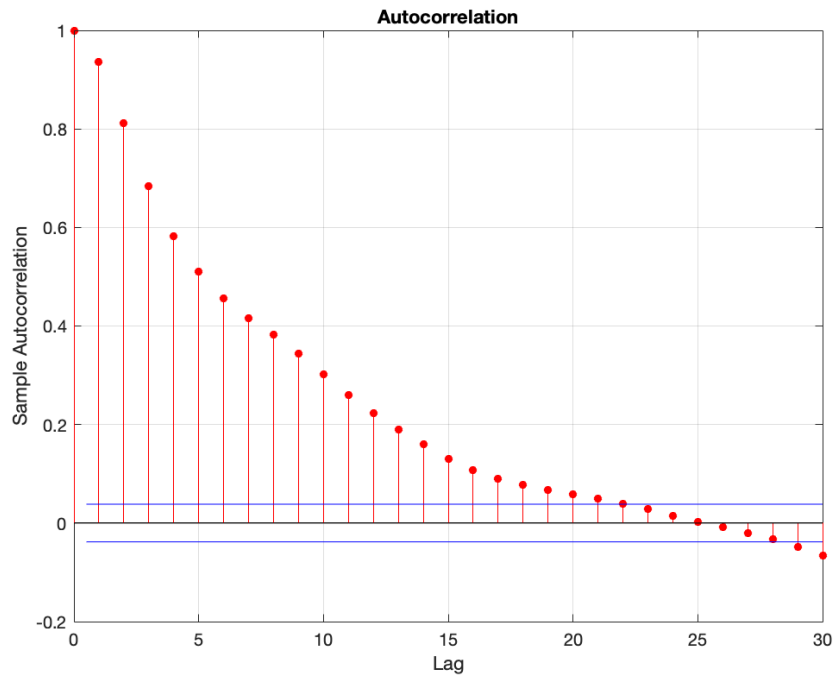
Figure A-5: Autocorrelation of measured coloured noise in the jackal for the rotational velocity in experiment 6 at input velocity v1
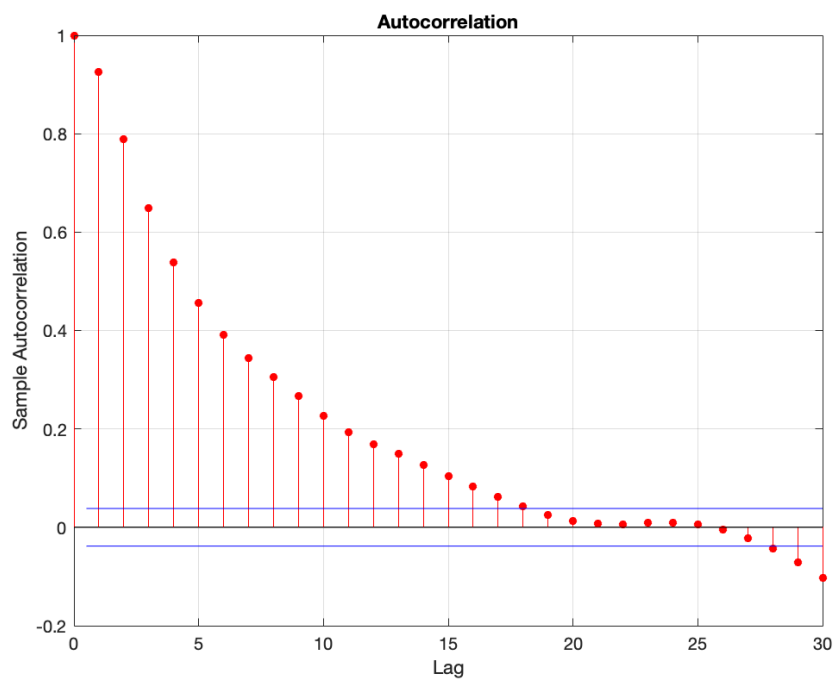
Figure A-6: Autocorrelation of measured coloured noise in the jackal for the rotational velocity in experiment 7 at input velocity v1
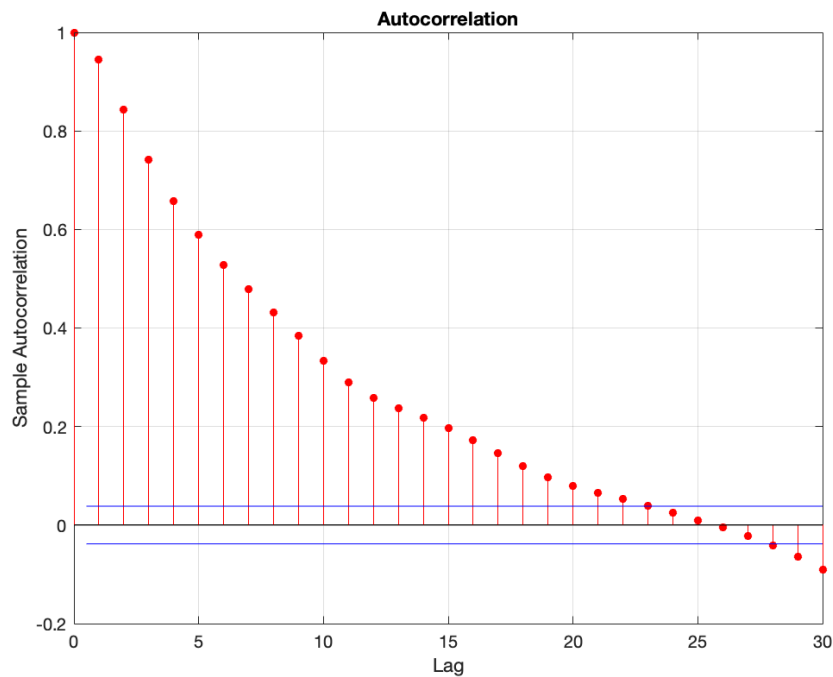
Figure A-7: Autocorrelation of measured coloured noise in the jackal for the rotational velocity in experiment 8 at input velocity v1
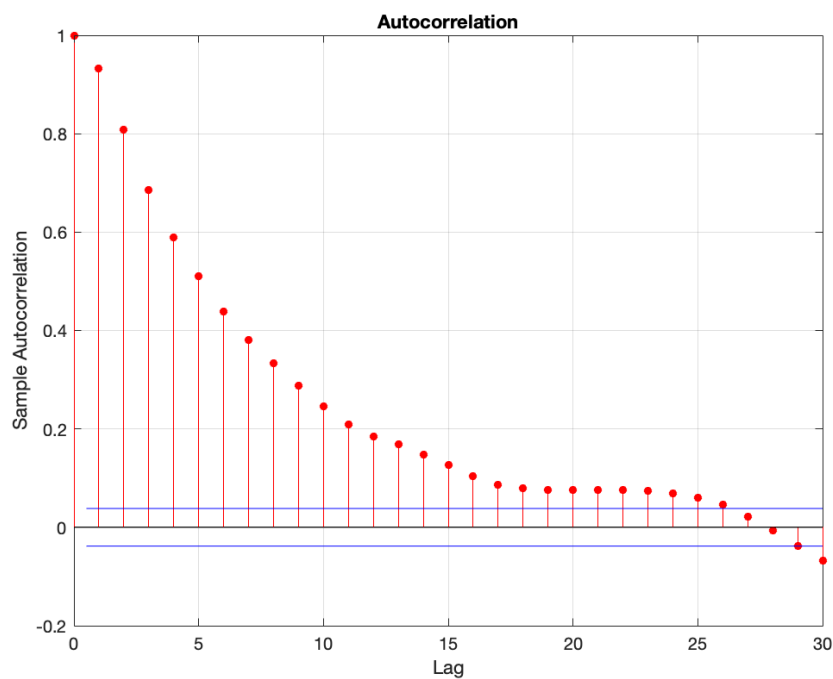
Figure A-8: Autocorrelation of measured coloured noise in the jackal for the rotational velocity in experiment 9 at input velocity v1
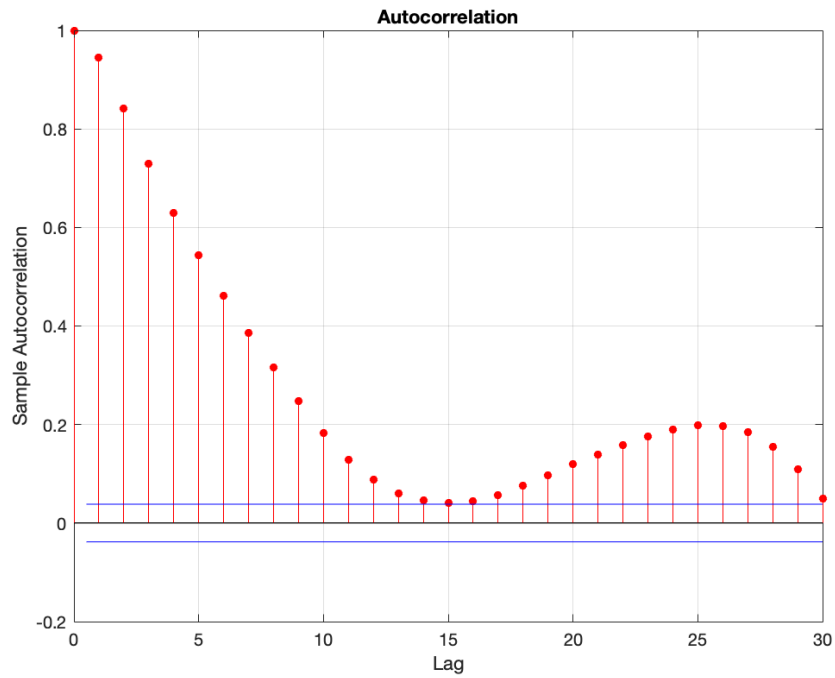
Figure A-9: Autocorrelation of measured coloured noise in the jackal for the rotational velocity in experiment 10 at input velocity v1
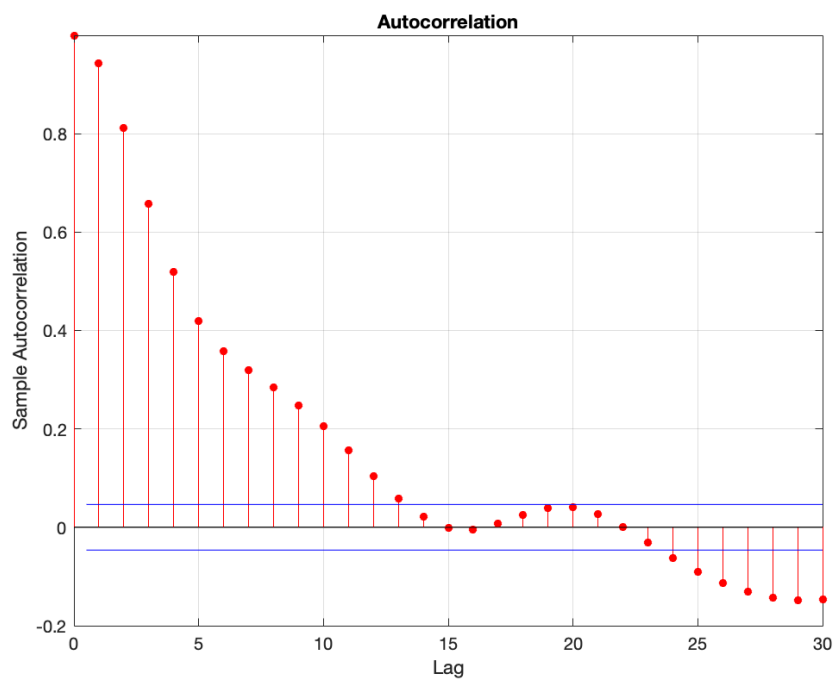
Figure A-10: Autocorrelation of measured coloured noise in the jackal for the rotational velocity in experiment 12 at input velocity v2
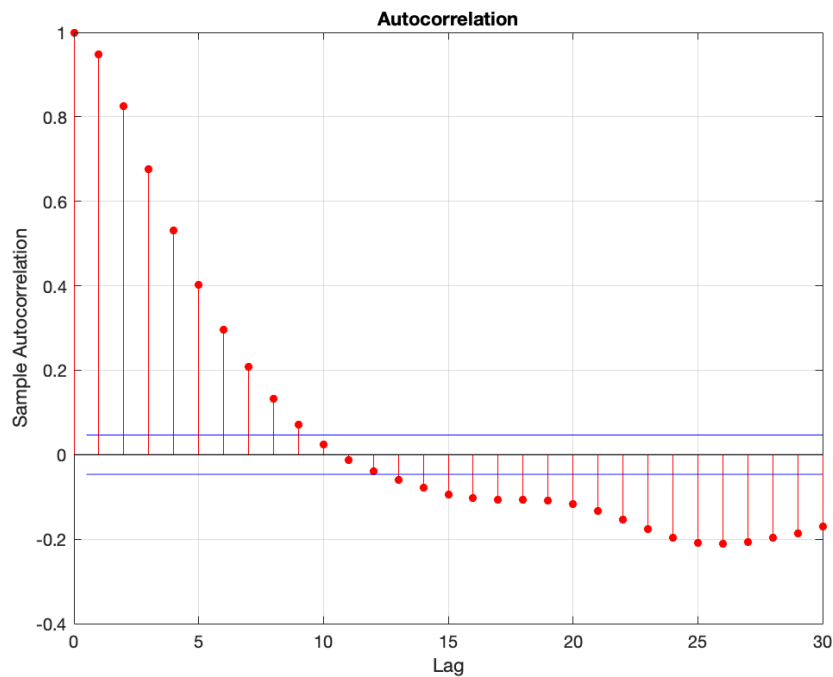
Figure A-11: Autocorrelation of measured coloured noise in the jackal for the rotational velocity in experiment 13 at input velocity v2
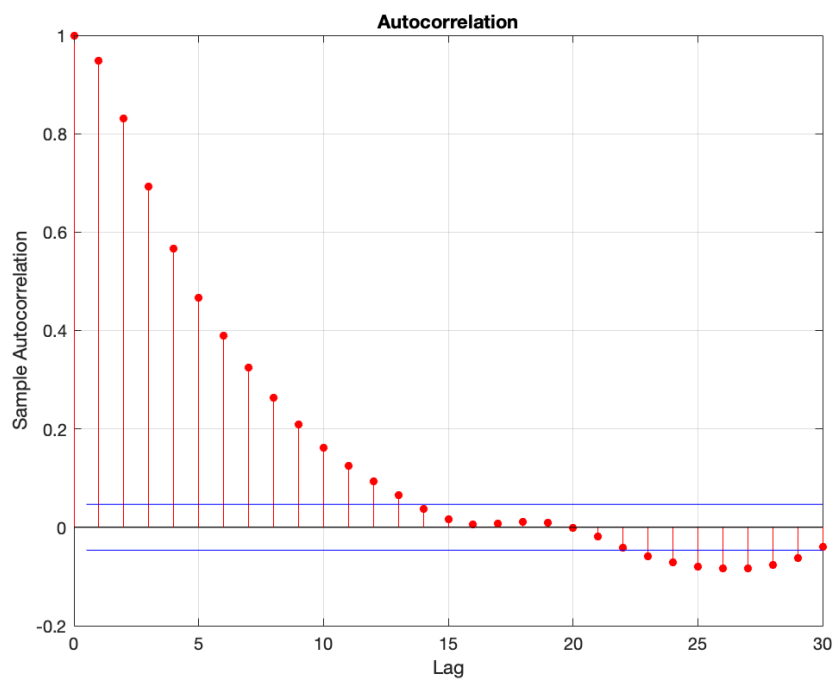
Figure A-12: Autocorrelation of measured coloured noise in the jackal for the rotational velocity in experiment 14 at input velocity v2
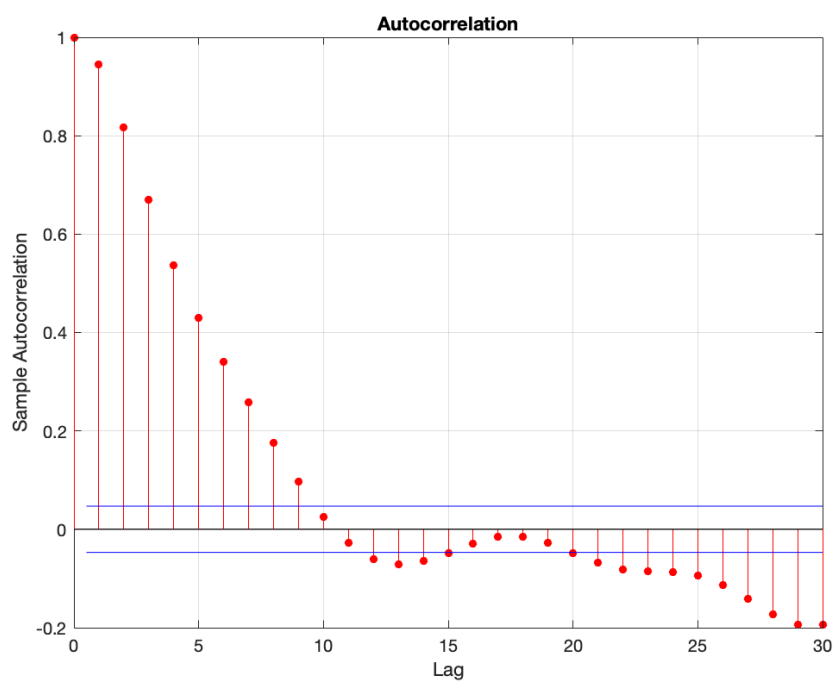
Figure A-13: Autocorrelation of measured coloured noise in the jackal for the rotational velocity in experiment 15 at input velocity v2

Bibliography

[1] K. Friston, "Friston, k.j.: The free-energy principle: a unified brain theory? nat. rev. neurosci. 11, 127-138," *Nature reviews. Neuroscience*, vol. 11, pp. 127–38, 02 2010.

[2] N. Y. E. E. Dan Ellis, Columbia University, "Coloured noise."

[3] M. Juriaan von Asmuth, Freddy Bos and Laurien Stubbe, "Colored noise in the slip patterns of a jackal robot," tech. rep., TU Delft, 06 2019.

[4] C. Robotics., "Jackal robot," August 2015.

[5] O. R. Foundation, "Ros."

[6] C. Robotics, "urdf-jackal."

[7] T. Keviczky, "Nerdlab."

[8] T. Wang, Y. Wu, J. Liang, C. Han, J. Chen, and Q. Zhao, "Analysis and experimental kinematics of a skid-steering wheeled robot based on a laser scanner sensor," *Sensors*, vol. 15, pp. 9681–9702, 05 2015.

[9] W. Yu, O. Y. Chuy, Jr., E. G. Collins, Jr., and P. Hollis, "Analysis and experimental verification for dynamic modeling of a skid-steered wheeled vehicle," *IEEE Transactions on Robotics*, vol. 26, pp. 340–353, April 2010.

[10] X. Wu, M. Xu, and L. Wang, "Differential speed steering control for four-wheel independent driving electric vehicle," in *2013 IEEE International Symposium on Industrial Electronics*, pp. 1–6, May 2013.

[11] H. Zamanian and F. Javidpour, "Dynamic modeling and simulation of 4-wheel skid-steering mobile robot with considering tires longitudinal and lateral slips," *International Journal of Scientific Research in Knowledge*, vol. 4, pp. 40–55, 02 2016.

[12] B. Magyar, "diff-drive-controller."

[13] G. Rill, *Road Vehicle Dynamics: Fundamentals and Modeling.* CRC Press, sept 2011. Series: Ground Vehicle Engineering.

[14] J. Deur, "Modeling and analysis of longitudinal tire dynamics based on the lugre friction model," *IFAC Proceedings Volumes*, vol. 34, no. 1, pp. 91 – 96, 2001. 3rd IFAC Workshop on Advances in Automotive Control 2001, Karlsruhe, Germany, 28-30 March 2001.

[15] Mathworks, "Pacejka in matlab."

[16] M. Wisse, "Derivation of generalised covariance matrix (not published)," tech. rep., TU Delft, 06 2019.

[17] N. Z. The University of Auckland, "Gaussian filtering."

[18] M. Galarnyk, "Explaining the 68-95-99.7 rule for a normal distribution."

[19] C A GLASBEY and G W HORGAN, "Image analysis for the biological sciences," tech. rep., Edinburgh, 02 1994.